7.1 Introduction

In this chapter the production of induced radioactivity at accelerators is described. This discussion begins with a review of the basic principles of the production of radioactivity. It proceeds with a discussion of the activation of accelerator components including some generalizations that may be used for practical health physics applications.

7.2 Fundamental Principles of Induced Radioactivity

In principle, induced radioactivity can be produced at all accelerators capable of liberating neutrons and other hadrons. When the accelerated beam strikes a nucleus, it can convert it into a different nuclide, which may, or may not, be radioactive. The **activity** of a given radionuclide refers to the number of atoms that decay per unit time. The customary unit of activity is the **Curie** (Ci), and its submultiples, historically defined to be the activity of 1 gram of natural radium and now precisely defined as 3.7 x 10^{10} decays per second. The SI unit of activity is the **Becquerel** (Bq), which is defined to be 1 decay per second, and its multiples. A related quantity of considerable importance is the **specific activity** that is defined to be the activity per unit volume (e.g., Bq cm^{-3}) or, alternatively, the activity per unit mass (e.g., Bq g^{-1}).

Radioactive decay is a random process characterized by a **mean-life** (units of time) denoted by τ, and its reciprocal (units of inverse time), the **decay constant**[1] λ, [$\lambda = 1/\tau$]. If a total of $N_{tot}(t)$ atoms of a radionuclide are present at time t, the total activity $A_{tot}(t)$ is determined by the random nature of radioactive decay to be

$$A_{tot}(t) = -\frac{dN_{tot}(t)}{dt} = \frac{1}{\tau} N_{tot}(t) = \lambda N_{tot}(t) . \qquad (7.1)$$

If at time $t = 0$ $N_{tot}(0)$ atoms are present, then this simple differential equation has the solution at some time $t = T$, [with $T > 0$]:

$$A_{tot}(T) = \lambda N_{tot}(0) \exp(-\lambda T) = A_{tot}(0) \exp(-\lambda T) . \qquad (7.2)$$

Often, the time required to decay to half of the original activity is tabulated. This **half-life**, denoted as $t_{1/2}$, is related to the mean-life by the following:

$$\tau = \frac{1}{\ln 2} t_{1/2} = \frac{1}{0.693} t_{1/2} = 1.442 t_{1/2} . \qquad (7.3)$$

[1] Care needs to be taken with respect to the usage of the symbol λ. In the literature and in this text it is, at different points, used for both the attenuation length and for the decay constant. The reader needs to take note of the context to apply the correct meaning.

The most simple activation situation at accelerators is illustrated by the steady irradiation of some material by a spatially uniform flux density of particles that begins at some time $t = 0$ and continues at a constant rate for an **irradiation period** that ends at $t = t_i$. This is followed by a decay period called the **cooling time** that is denoted t_C, a period of time that begins at $t = t_i$ and ends at $t = t_i + t_C$. For this simple situation, self-absorption of the hadrons by the target is ignored, as is the fact that a whole spectrum of particles might be incident. Thus the process of producing the radioactivity is characterized by a single average cross section, σ. In the more complicated generalized situations the value of this cross section must be obtained from averaging over an energy spectrum.

The number of atoms of the radionuclide of interest per unit volume will thus be governed by the following equation during the period of the irradiation:

$$\frac{dn(t)}{dt} = -\lambda n(t) + N\sigma\phi, \tag{7.4}$$

where $n(t)$ is the number density of atoms of the radionuclide of interest at time t (cm^{-3}). N is the number density of "target" atoms (cm^{-3}), σ is in units of cm^2, and ϕ is the flux density ($cm^{-2}\ sec^{-1}$) of incident particles. On the right hand side of the above equation, the first term represents the loss of radionuclides through decay during the irradiation while the second term represents the gain of radionuclides through the production reaction under consideration. The equation has the following solution for $0 < t < t_i$:

$$n(t) = \frac{N\sigma\phi}{\lambda}\left(1 - e^{-\lambda t}\right). \tag{7.5}$$

Thus the specific activity induced in the material as a function of time during the irradiation is given by $a(t) = \lambda\, n(t)$, hence

$$a(t) = N\sigma\phi\left(1 - e^{-\lambda t}\right)\ (\text{Bq cm}^{-3}) \quad \text{for } 0 < t < t_i. \tag{7.6}$$

To obtain specific activity in units of Curies cm^{-3}, one must simply divide the resulting value by the conversion factor 3.7×10^{10} Bq $Curie^{-1}$. At the instant of completion of the irradiation ($t = t_i$), the specific activity will thus be:

$$a(t_i) = N\sigma\phi\left\{1 - \exp(-\lambda t_i)\right\}\ (\text{Bq cm}^{-3}), \tag{7.7}$$

so that the specific activity as a function of time is characterized by a buildup from zero to the saturation value of $N\sigma\phi$ for infinitely long irradiations. After the irradiation has ceased ($t > t_i$), the specific activity as a function of the cooling time, t_C, will obviously

decay exponentially and be given by

$$a(t_c) = N\sigma\phi\{1-\exp(-\lambda t_i)\}\{\exp(-\lambda t_c)\}\ (\text{Bq/cm}^3), \tag{7.8}$$

where t_C is the cooling time; $t_C = t - t_i$. (7.9)

For total activities in situations where uniform flux densities of particles of constant energy are incident on a homogeneous "target", one can simply multiply by the volume of the "target"; or in more complex cases involving non-uniform flux densities, one can integrate the above over the various sub-volumes of the target.

For γ-ray emitters typical of those emitted by accelerator-produced radionuclides in the range of from about 100 keV to 10 MeV, many textbooks in health physics demonstrate that the absorbed dose rate, *dD/dt* (rad h^{-1}), at a distance *r* (meters) from a "point" source is given in terms of the source strength, *S*, (Ci), and the photon energy, E_γ(MeV) by

$$\frac{dD}{dt} = 0.4\frac{S}{r^2}\sum_i E_{\gamma i}\ . \tag{7.10}$$

The summation is over all γ-rays present, including appropriate branching fractions if multiple photons are emitted in the course of decay. If *dD/dt* is desired as an approximate absorbed dose rate in Gy h^{-1} at a distance, *r* (meters), from a source strength *S* in gigaBecquerels[2] (GBq), the constant 0.4 becomes 1.08 x 10^{-4}. One can use the above to determine the absorbed dose rate from a given activated object if it is a point source. For non-point sources, an appropriate spatial integration must be performed.

7.3 Activation of Components at Electron Accelerators

7.3.1 General Phenomena

At electron accelerators, as was described in Chapter 3, the direct interactions of electrons in material results in the copious production of photons. Through various nuclear reaction channels, these photons then proceed to produce charged particles and neutrons that then interact further with material to produce radioactivity. In general, if the facility is properly shielded against prompt radiation, the radioactivity hazard will be confined to accelerator components and the interior of the accelerator enclosure. The experience at most accelerators bears this out. The vast majority of the radiation exposure incurred by the workers is due to maintenance activities on radioactivated components, handling and

[2] The GBq (10^9 Bq) is often a better unit of activity for practical work than is the Bq.

moving of activated items, radiation surveys, and radioactive waste handling rather than to exposure to the prompt radiation fields. An understanding of the production of radionuclides can help reduce personnel exposures through the selection of more appropriate machine component materials and the optimization of decay ("cool-down") times recommended after the beam has been turned off. Some familiarity with the relevant cross sections is extremely useful. Global data has been compiled by Barbier (Ba69). These data are given Figs. 7.1, 7.2, and 7.3. Fig. 7.1 presents data in the form of contour plots of the cross sections $\sigma(E_\gamma, A_T)$ where E_γ is the photon energy and A_T is the atomic mass number of the target material. Figs. 7.2 and 7.3 provide the cross sections for specific processes as a function of energy. These data are intended to convey the general idea of the importance of various processes at different energies. Specific data should be researched in the literature if precise, accurate calculations are desired.

7.3.2 Results for Electrons at Low Energies

Results such as those presented in Section 7.3.1 form the basis of detailed activation calculations. Swanson (Sw79a) utilized the methodology of "Approximation B" of the analytical shower theory of Rossi and Griesen (Ro41), mentioned in Section 3.4.1, to estimate saturation activities rates in various materials. Since the energy domain below about 35 MeV is characterized by rapidly varying cross sections, Swanson provided energy-dependent results. Here only reactions of the type (γ, n), (γ, p), (γ, np), and (γ, 2n) were considered. Other reactions were ignored due to higher energy thresholds and small cross sections. Swanson points out that the dependence of the induced activity as a function of energy will generally follow that of the neutron yields (see Fig. 3.7). In Swanson's calculations, the material in question absorbs *all* of the beam power and has been irradiated for an *infinite* time with no cooldown [$t_i = \infty$, $t_c = 0$ in Eq. (7.8)]. Thus, so-called **saturation activities** are calculated, normalized to the incident electron beam power (kW). Results of these calculations, taking into account the isotopic natural abundances found in the target materials and the specific reaction thresholds, are provided in Table 7.1. According to Swanson, the results are probably accurate to about $\pm$ 30 per cent. At these low energies, the distribution of the radioactivity can often approximately be taken to be that of a point source for purpose of calculating the residual absorbed dose rates using, for example, Eq. (7.10) taking the summation over all of the γ-ray emitters presented at a given time. Table 7.1 thus provides the **specific gamma constants**, Γ, for each tabulated radionuclide. These constants connect activity with the **exposure rates** at a distance of one meter assuming point source conditions and accounting for all the photons emitted by the decaying radionuclide, even those emitted secondarily such as internal bremsstrahlung and annihilation radiation due to β^+ emission manifested in the form of a pair of 0.511 MeV photons. For approximate point sources, exposure rates at other distances can be calculated by incorporating the inverse square law. The units of **exposure rate** (R h^{-1}) are tied to the rate of liberation of ions in air by photons. One R h^{-1} is the hourly liberation of one electrostatic unit of charge and is approximately equivalent to one rad h^{-1} of **absorbed dose** in tissue placed in the radiation field under consideration in such photon radiation fields.

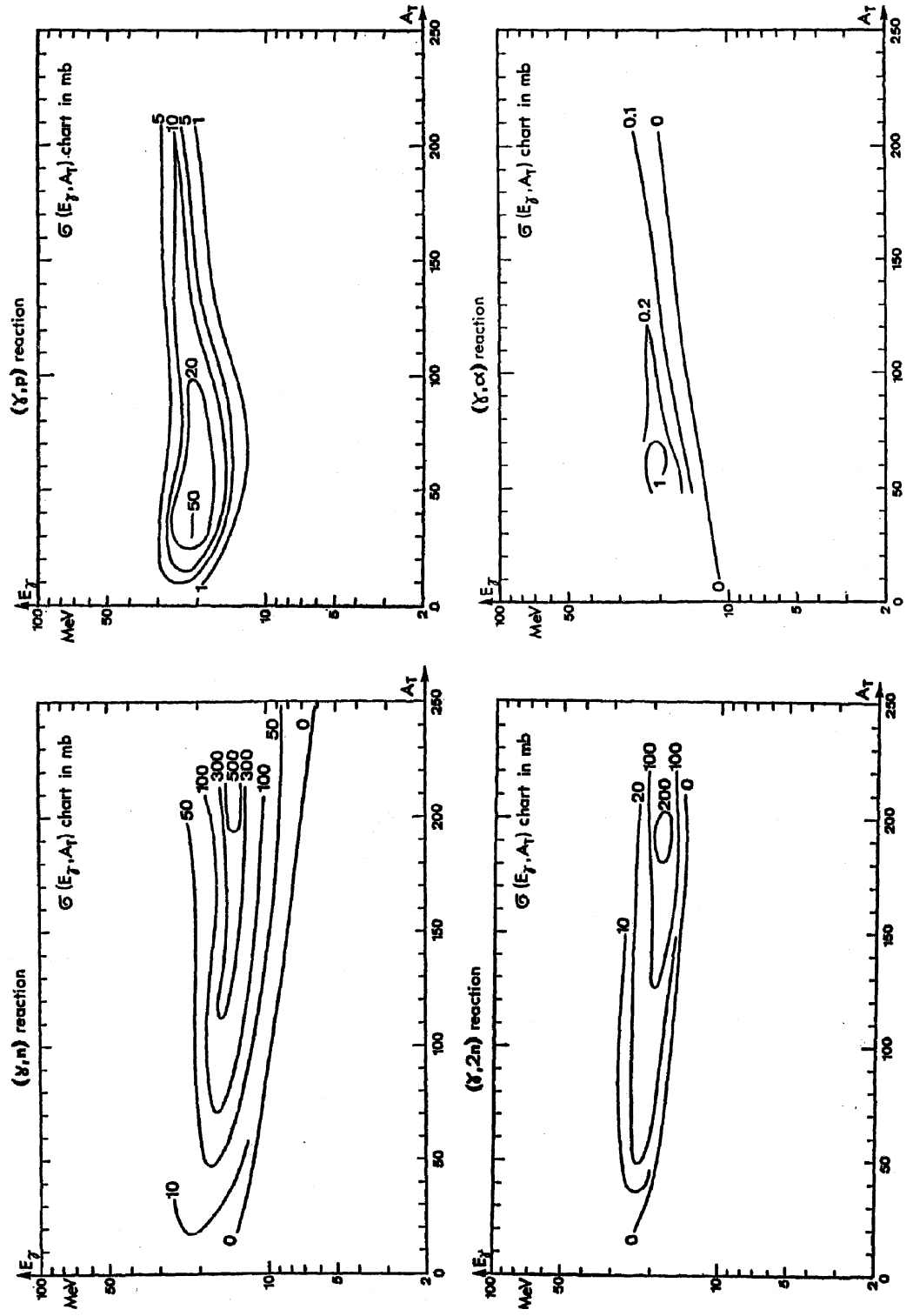

Fig. 7.1 Contours of equal cross section for photon-induced nuclear reactions (γ, n), (γ, p), (γ, 2n), and (γ, α) as a function of photon energy, E_γ, and target material mass number, A_T. The results have been smoothed in these plots. [Adapted from (Ba69).]

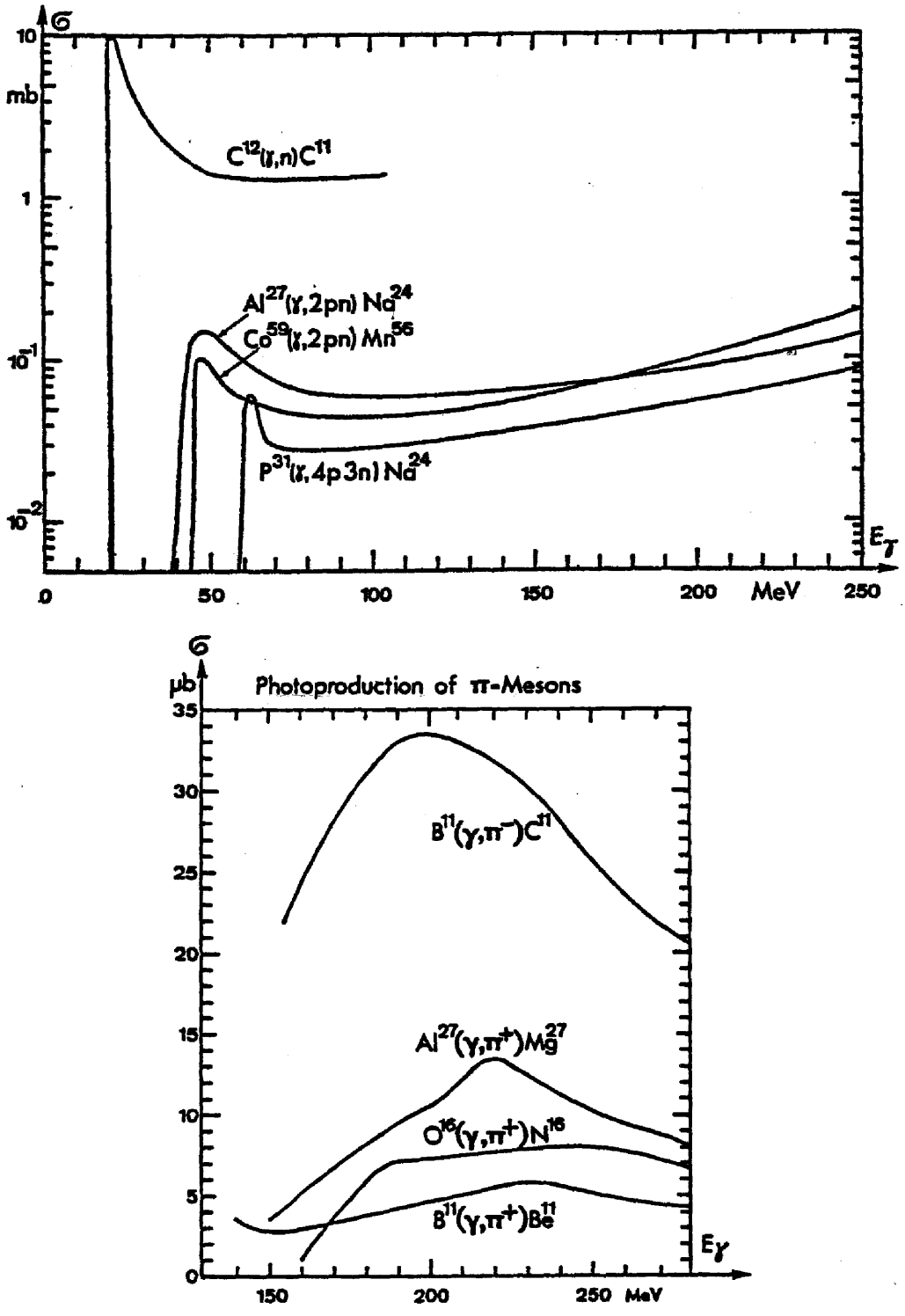

Fig. 7.2 Values of cross sections for important photon-induced reactions (upper) and for photo-pion reactions at intermediate energies. [Adapted from (Ba69).]

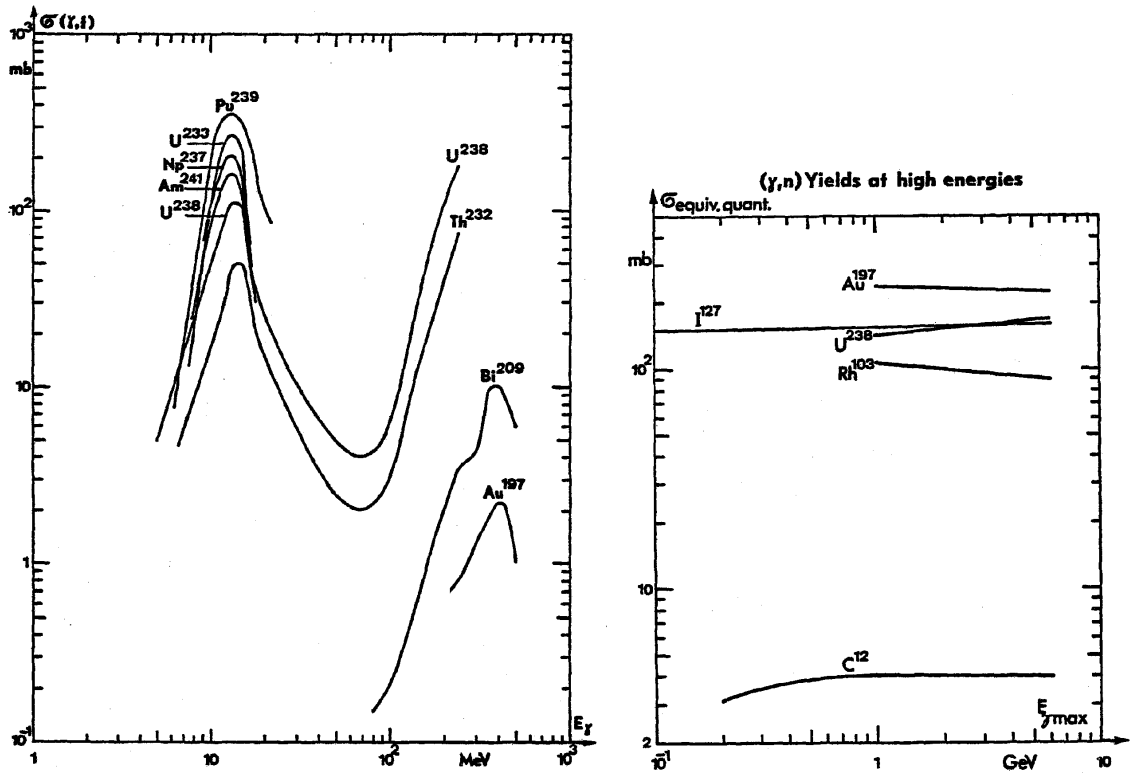

Fig. 7.3 Values of cross sections for photofission (γ, f) and photoneutron (γ, n) reactions at intermediate and high energies for photons incident on a variety of materials. [Adapted from (Ba69).]

Table 7.1 Calculations of saturation activities per unit beam power (Ci kW^{-1}) and saturation exposure rates at one meter, Γ, for electrons of energy E_o incident on various target materials. [Adapted from (Sw79a).]

Target material	Radionuclide	$T_{\frac{1}{2}}$	Threshold (MeV)	Γ[a] ((R·h⁻¹)(Ci·m⁻²)⁻¹)	Saturation activity (Ci·kW⁻¹)[b] Accelerator energy E_0 (MeV) 10	15	20	25	30	35
Al	Na-24	14.96 h	23.71	1.83	–	–	–	0.0005	0.010	0.03
	Al-26m	6.37 s	13.03	0.59	-	0.02	1.0	3.8	6.6	8.8
Fe	Mn-54	303 d	20.42	1.20	–	–	–	0.16	0.45	0.59
	Mn-56	2.576 h	10.57	0.86	–	0.003	0.014	0.024	0.030	0.032
	Fe-53	8.51 min	13.62	0.67	–	0.01	0.26	0.52	0.67	0.74
Ni	Ni-56	6.10 d	22.5	1.58 } c	-	–	–	0.003	0.034	0.066
	Co-56	77.3 d	–	2.27 }						
	Ni-57	36.0 h	12.19	1.35 } c		0.10	1.2	2.6	3.6	4.2
	Co-57	270 d	–	1.29 }						
Cu	Cu-61	3.32 h	19.73	0.71	–	–	$\sim 10^{-4}$	0.23	0.65	0.87
	Cu-62	9.76 min	10.84	0.60	–	0.77	4.8	8.6	11.	11.
	Cu-64	12.80 h	9.91	0.38	$\sim 10^{-5}$	0.62	2.8	4.2	4.8	5.0
W	Ta-182	16.5 min	7.15	0.15 }	0.017	0.17	0.31	0.35	0.36	0.36
		115.1 d		0.61 }						
	Ta-183	5.0 d	7.71	0.15	0.027	0.34	0.56	0.61	0.62	0.63
	W-181	140 d	7.99	0.09	0.27	4.0	7.6	8.6	8.9	9.1
	W-185	1.62 min	7.27	0.18 }	0.47	4.5	7.3	7.9	8.1	8.1
		75 d		no γ }						
Au	Au-195	30.6 s	14.80	0.15 }		$<10^{-3}$	2.0	4.3	5.3	5.5
		183 d		0.07 }						
	Au-196	9.7 h	8.07	0.11)	1.5	20.	35.	39.	40.	41.
		6.18 d		0.29)						
Pb	Pb-203	52.1 h	8.38	0.18	0.013	0.22	0.41	0.45	0.46	0.47
	Pb-204m	66.9 min	14.85	1.14		$<10^{-4}$	0.33	0.74	1.0	1.2

[a] Where two values are given, the first is for the metastable state.
[b] Activity per incident electron beam power.
[c] The first nuclide is parent of the second.

7.3.3 Results for Electrons at High Energies

For higher energy electrons, more reaction channels become available but the energy dependence is diminished. Swanson has also provided calculations of the production of radionuclides in this energy domain and the results are provided here in Table. 7.2 (Sw79a). The results are valid (to within a factor of two) for any beam energy E_o at least somewhat above the nuclide production threshold. Specific gamma constants for point source conditions, Γ, reaction thresholds, and integral radionuclide production cross sections summed over parent isotopes per MeV of electron beam energy, $\Sigma f\sigma_{-2}$ are

Table 7.2 Calculations of saturation activities (Ci kW^{-1}) and saturation exposure rates at one meter, Γ, in various materials for high energy electrons. [Adapted from (Sw79a).]

Material: Natural aluminium[a]

Daughter nuclide				Dominant production			Cross-section[c]		A_s[e] Saturation activity (Ci·kW^{-1})	$\dot{X}_s$[f] Saturation exposure rate ((R·h^{-1})(kW·m^{-2})$^{-1}$)
Nuclide	$T_{\frac{1}{2}}$		Γ[b] ((R·h^{-1})(Ci·m^{-2})$^{-1}$)	Parent isotope	Type	Threshold (MeV)	$\Sigma f\sigma_{-2}$ (μb·MeV^{-1})	Note[d]		
Be-7	53.6	d	0.029	Al-27	(γ,sp)	32.95	2.3	S	0.13	0.004
C-11	20.34	min	0.59	Al-27	(γ,sp)	33.53	1.0	S	0.051	0.03
N-13	9.96	min	0.59	Al-27	(γ,sp)	25.56	0.3	S	0.013	0.008
O-15	123	s	0.59	Al-27	(γ,sp)	33.43	1.4	S	0.067	0.04
F-18	109.7	min	0.58	Al-27	(γ,sp)	34.39	2.8	S	0.14	0.08
Ne-24	3.38	min	0.31	Al-27	(γ,3p)	33.11	0.07	S	0.0031	0.001
Na-22	2.62	a	1.19	Al-27	(γ,3n2p)	22.51	4.7	S	0.25	0.30
Na-24	14.96	h	1.83	Al-27	(γ,1n2p)	23.71	5.4	S	0.28	0.51
Al-25	7.24	s	0.59	Al-27	(γ,2n)	24.41	0.75	S	0.039	0.023
Al-26	7.4×10^5	a	1.38	Al-27	(γ,n)	13.03	420	B	8.8	6.0 g
Al-26m	6.37	s	0.59							2.6 g
Mg-27[i]	9.46	min	0.49	Al-27	(γ,π$^+$)	≈140	0.3	S	0.016	0.008

Material: Natural iron[a]

Daughter nuclide				Dominant production			Cross-section[c]		A_s[e] Saturation activity (Ci·kW^{-1})	$\dot{X}_s$[f] Saturation exposure rate ((R·h^{-1})(kW·m^{-2})$^{-1}$)
Nuclide	$T_{\frac{1}{2}}$		Γ[b] ((R·h^{-1})(Ci·m^{-2})$^{-1}$)	Parent isotope	Type	Threshold (MeV)	$\Sigma f\sigma_{-2}$ (μb·MeV^{-1})	Note[d]		
Sc-46	83.9	d	1.09	Fe-54	(γ,sp)	37.41	(15)	E	(0.2)	(0.2)
V-48	16.0	d	1.95	Fe-54	(γ,sp)	25.86	30	D*	(0.4)	(0.8)
Cr-51	27.8	d	0.76	Fe-54	(γ,sp)	19.74	(30)	E	(0.4)	(0.3)
Mn-52	5.60	d	2.18	Fe-54	(γ,np)	20.89		B	0.036	0.039 g
Mn-52m	21.1	min	1.30							0.023 g
Mn-54	303	d	1.20	Fe-56	(γ,np)	20.42		B	0.59	0.70
Mn-56	2.576	h	0.86	Fe-57	(γ,p)	10.57		B	0.032	0.027
Fe-52[j]	8.2	h	0.72	Fe-54	(γ,2n)	24.06		B	0.056	0.040
Fe-53	8.51	min	0.67	Fe-54	(γ,n)	13.62		B	0.74	0.49
Fe-55	2.60	a	0.69	Fe-56	(γ,n)	11.21		B	13.3	9.0
Fe-59[h]	45.6	d	0.62	Fe-58	(n,γ)	–		–	–	–[h]

Material: Natural nickel[a]

Daughter nuclide				Dominant production			Cross-section[c]		A_s[e] Saturation activity (Ci·kW^{-1})	$\dot{X}_s$[f] Saturation exposure rate ((R·h^{-1})(kW·m^{-2})$^{-1}$)
Nuclide	$T_{\frac{1}{2}}$		Γ[b] ((R·h^{-1})(Ci·m^{-2})$^{-1}$)	Parent isotope	Type	Threshold (MeV)	$\Sigma f\sigma_{-2}$ (μb·MeV^{-1})	Note[d]		
Ni-56	6.10	d	1.58	Ni-58	(γ,2n)	22.45		B	0.1	0.16
Co-56[k]	77.3	d	2.27						0.1	0.22
Ni-57	36.0	h	1.35	Ni-58	(γ,n)	12.19		B	5.9	7.9
Co-57[k]	270	d	1.29						5.9	7.5
Co-60	5.263	a	1.30	Ni-61	(γ,p)	9.86			(0.1)	(0.1)

Table 7.2-continued

Material: Natural copper[a]

Daughter nuclide				Dominant production			Cross-section[c]		A_s[e] Saturation activity ($Ci \cdot kW^{-1}$)	$\dot{X}_s$[f] Saturation exposure rate $((R \cdot h^{-1})(kW \cdot m^{-2})^{-1})$
Nuclide	$T_{\frac{1}{2}}$		Γ[b] $((R \cdot h^{-1})(Ci \cdot m^{-2})^{-1})$	Parent isotope	Type	Threshold (MeV)	$\Sigma f\sigma_{-2}$ ($\mu b \cdot MeV^{-1}$)	Note[d]		
Co-58	71.3	d	1.13	Cu-63	(γ,sp)	41.75		Sa	~0.66	0.37 g
Co-58m	9.2	h	0.65							0.21 g
Co-60	5.263	a	1.30	Cu-63	(γ,n2p)	18.86		Sa	0.65	0.83
Ni-63	92	a	no γ	Cu-65	(γ,np)	17.11		B	0.45	no γ
Cu-61	3.32	h	0.71	Cu-63	(γ,2n)	19.73		B	0.87	0.61
Cu-62	9.76	min	0.60	Cu-63	(γ,n)	10.84		B	11.	6.5
Cu-64	12.80	h	0.38	Cu-65	(γ,n)	9.91		B	5.0	1.9
Cu-66[h]	5.10	min	0.052	Cu-65	(n,γ)	–		–	–	– [h]

Material: Natural tungsten[a]

Daughter nuclide				Dominant production			Cross-section[c]		A_s[e] Saturation activity ($Ci \cdot kW^{-1}$)	$\dot{X}_s$[f] Saturation exposure rate $((R \cdot h^{-1})(kW \cdot m^{-2})^{-1})$
Nuclide	$T_{\frac{1}{2}}$		Γ[b] $((R \cdot h^{-1})(Ci \cdot m^{-2})^{-1})$	Parent isotope	Type	Threshold (MeV)	$\Sigma f\sigma_{-2}$ ($\mu b \cdot MeV^{-1}$)	Note[d]		
Ta-180m	8.15	h	0.038	W-182	(γ,np)	14.66		B	0.049	0.001[g]
Ta-182m	16.5	min	0.15	W-183	(γ,p)	7.15		B	0.36	0.027 g
Ta-182	115.1	d	0.61							0.11 g
Ta-183	5.0	d	0.15	W-184	(γ,p)	7.71		B	0.62	0.09
Ta-184	8.7	h	0.84	W-186	(γ,np)	14.91		B	0.048	0.04
Ta-185	50	min	0.11	W-186	(γ,p)	8.39		B	0.56	0.062
W-181	140	d	0.09	W-182	(γ,n)	7.99		B	8.9	0.80
W-183m	5.3	s	0.11	W-184	(γ,n)	7.42		B	8.6	0.43[g]
W-185	75	d	no γ	W-186	(γ,n)	7.27		B	8.1	no γ
W-185m	1.62	min	0.18							0.73 g
W-187[h]	23.9	h	0.26	W-186	(n,γ)	–		–	–	– [h]

Material: Natural gold[a]

Daughter nuclide				Dominant production			Cross-section[c]		A_s[e] Saturation activity ($Ci \cdot kW^{-1}$)	$\dot{X}_s$[f] Saturation exposure rate $((R \cdot h^{-1})(kW \cdot m^{-2})^{-1})$
Nuclide	$T_{\frac{1}{2}}$		Γ[b] $((R \cdot h^{-1})(Ci \cdot m^{-2})^{-1})$	Parent isotope	Type	Threshold (MeV)	$\Sigma f\sigma_{-2}$ ($\mu b \cdot MeV^{-1}$)	Note[d]		
Pt-195m	4.1	d	0.08	Au-197	(γ,np)	13.74		B	0.10	0.008
Au-195	183	d	0.07	Au-197	(γ,2n)	14.80		B	5.5	0.19 g
Au-195m	30.6	s	0.15							0.41 g
Au-196	6.18	d	0.29	Au-197	(γ,n)	8.07		B	41	5.9 g
Au-196m	9.7	h	0.11							2.3 g
Au-198[h]	2.697	d	0.23	Au-197	(n,γ)	–		–	–	– [h]

Table 7.2-continued

Material: Natural lead[a]

Daughter nuclide			Dominant production			Cross-section[c]		A_s[e] Saturation activity ($Ci \cdot kW^{-1}$)	$\dot{X}_s$[f] Saturation exposure rate $((R \cdot h^{-1})(kW \cdot m^{-2})^{-1})$
Nuclide	$T_{\frac{1}{2}}$	Γ[b] $((R \cdot h^{-1})(Ci \cdot m^{-2})^{-1})$	Parent isotope	Type	Threshold (MeV)	$\Sigma f \sigma_{-2}$ ($\mu b \cdot MeV^{-1}$)	Note[d]		
Tl-204	3.81 a	no γ	Pb-206	(γ,np)	14.83		B	0.025	–
Tl-206	4.19 min	no γ	Pb-207	(γ,p)	7.46		B	1.0	–
Tl-207m	1.3 s	0.74	Pb-208	(γ,p)	8.04		B	2.5	0.91 g
Tl-207	4.79 min	8×10^{-4}							0.001 g
Pb-202m	3.62 h	1.16	Pb-204	(γ,2n)	15.32		B	0.06	0.03 g
Pb-202	3.0×10^5 a	–							–
Pb-203m	6.1 s	0.33	Pb-204	(γ,n)	8.38		B	0.83	0.13 g
Pb-203	52.1 h	0.18							0.07 g
Pb-204m	66.9 min	1.14	Pb-206	(γ,2n)	14.85		B	2.4	1.4 g
Pb-204	Stable	–							–

Material: Concrete[a]

Daughter nuclide			Dominant production			Assumed abundance of parent by weight (%)	A_s[d,e] Saturation activity ($Ci \cdot kW^{-1}$)	$\dot{X}_s$[f] Saturation exposure rate $((R \cdot h^{-1})(kW \cdot m^{-2})^{-1})$
Nuclide	$T_{\frac{1}{2}}$	Γ[b] $((R \cdot h^{-1})(Ci \cdot m^{-2})^{-1})$	Parent isotope	Type	Threshold (MeV)			
C-11	20.34 min	0.59	C-12	(γ,n)	18.72	0.10	3.5×10^{-3}	2.1×10^{-3}
O-15	123 s	0.59	O-16	(γ,n)	15.67	53	2.6	1.5
Na-22	2.62 a	1.19	Na-23	(γ,n)	12.44	1.6	0.1	0.12
Mg-23	12.1 s	0.62	Mg-24	(γ,n)	16.55	0.16	7.3×10^{-3}	4.5×10^{-3}
Al-26m	6.37 s	0.59	Al-27	(γ,n)	13.03	3.4	9.2×10^{-4}	5.4×10^{-4}
Si-27	4.14 s	0.59	Si-28	(γ,n)	17.18	31	2.0	1.2
K-38	7.71 min	1.56	K-39	(γ,n)	13.08	1.2	0.1	0.15
Fe-53	8.51 min	0.65	Fe-54	(γ,n)	13.62	0.08	1.0×10^{-4}	6.4×10^{-5}

[a] *Composition assumed* (%):
Concrete (by weight): (C-12, O-16, Na-23, Mg-24, Al-27, Si-28, K-39, Fe-54, others) = (0.10, 53.0, 1.6, 0.16, 3.4, 31.0, 1.2, 0.08, 9.5).
Aluminium: Al-27: 100%.
Iron: Fe-54: 5.84%, Fe-56: 91.68%, Fe-57: 2.17%, Fe-58: 0.31%.
Nickel: Ni-58: 67.76%, Ni-60: 26.16%, Ni-61: 1.25%, Ni-62: 3.66%, Ni-64: 1.16%.
Copper: Cu-63: 69.1%, Cu-65: 30.9%.
Tungsten: W-182: 26.4%, W-183: 14.4%, W-184: 30.6%, W-186: 28.4%.
Gold: Au-197: 100%.
Lead: Pb-204: 1.4%, Pb-206: 25.1%, Pb-207: 21.7%, Pb-208: 52.3%.

[b] Specific gamma-ray constant.
[c] Sum of the σ_{-2} for each parent isotope, weighted by the isotope fraction. This is given if Approximation A is used in the estimation of activity.
[d] Refers to source of data, see (Sw79a).
[e] Saturation activity per kW electron beam power.
[f] Exposure rate at 1 metre and per kW of electron beam power. The unit m^2 implies an inverse-square dependence on distance. Exposure rates not corrected for self-shielding or distribution of activity.
[g] Equal division between metastable and ground state assumed.
[h] (n,γ) reaction.
[i] Photopion reaction having threshold ~140 MeV.
[j] Decays to Mn-52m, then to Mn-52.
[k] Daughter of Ni isobar.

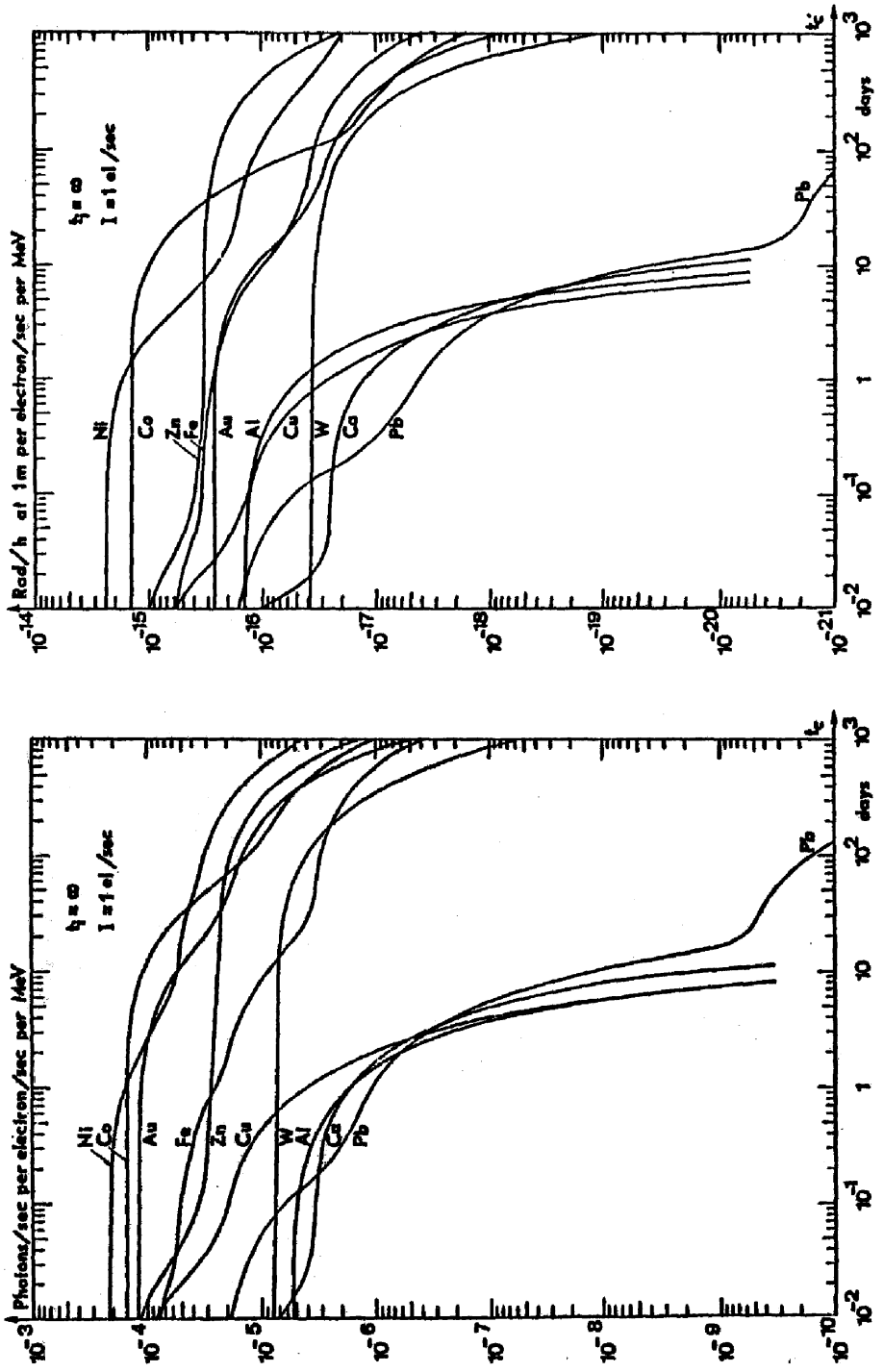

Fig. 7.4 Total photon emission rate (left) and absorbed dose rates (right) from radioactive nuclei produced in large targets of various materials irradiated by an electron current of 1 electron sec^{-1} per MeV incident electron energy as a function of time since the cessation of the irradiation. The irradiation was assumed to have occurred for an *infinitely* long period of time. The absorbed dose rates (right) are those found at 1 meter from a point source containing all of the radioactive nuclei. [Adapted from (Ba69).]

provided along with saturation activities and exposures rates. The beams are assumed to be totally absorbed in the material and no self-shielding effects are taken into account. The distribution of radioactivity within the material is not taken into account. The results are, again, presented for saturation conditions, i.e. $t_i = \infty$, $t_c = 0$ in Eq. (7.8), for the compositions of materials described in the footnotes to the table. Cooling curves have been reported by Barbier (Ba69) for high energy electrons incident on various materials for an infinite irradiation at the rate of one electron per second. The results are given in Fig. 7.4 per MeV of incident electron energy for an infinite irradiation time, t_i. In this figure, results are given for both the photon emission rates (photons s^{-1}) and for the exposure rates (rads hr^{-1}) per electron s^{-1} assuming the applicability of point source conditions. As discussed in Chapter 3, the simplicity and lack of strong energy dependence of the photoneutron spectra make these results possible.

7.4 Activation of Accelerator Components at Proton and Ion Accelerators

7.4.1 General Phenomena

Protons having energies above about 10 MeV, or sometimes less, will produce radioactivity. This will also occur for accelerators of other ions above a specific energy of about 10 MeV/nucleon. In some special cases radioactivity can be produced at much lower energies due to exothermic nuclear reactions that either produce radionuclides directly or emit neutrons capable of inducing radioactivity through their secondary interactions. As with electron accelerators, if a given accelerator is properly designed with respect to the shielding against prompt radiation and has proper access controls to avoid direct beam-on exposure to people, the induced radioactivity is very likely to be the dominant source of occupational radiation exposure.

For the lower incident energies, below about 30 MeV, one is first concerned with production of radionuclides by such processes as (p, γ) and single- and multi-nucleon transfer reactions. While the details of the total cross sections for such reactions are complex, the systematics and approximate energy dependencies are globally well understood. In general, one has endothermic nuclear reactions that have a threshold, E_{th}, below which the process is forbidden by conservation of energy. For nuclear reactions induced by ions, E_{th} is related to the reaction Q -value [see Eq. (4.1)], Q_v, by

$$E_{th} = \frac{m + M}{M}\left|Q_v\right|, \tag{7.11}$$

where Q_v is negative in an endothermic reaction that, thus, has a positive value of E_{th}. In this equation, m is the mass of the incident projectile while M is the mass of the target atom, assumed to stationary in the Laboratory frame of reference. The treatise by Barbier (Ba69) has rather adequately handled activation by all types of particles. As was the case with electrons, some of these results are in the form of contour plots of the cross sections

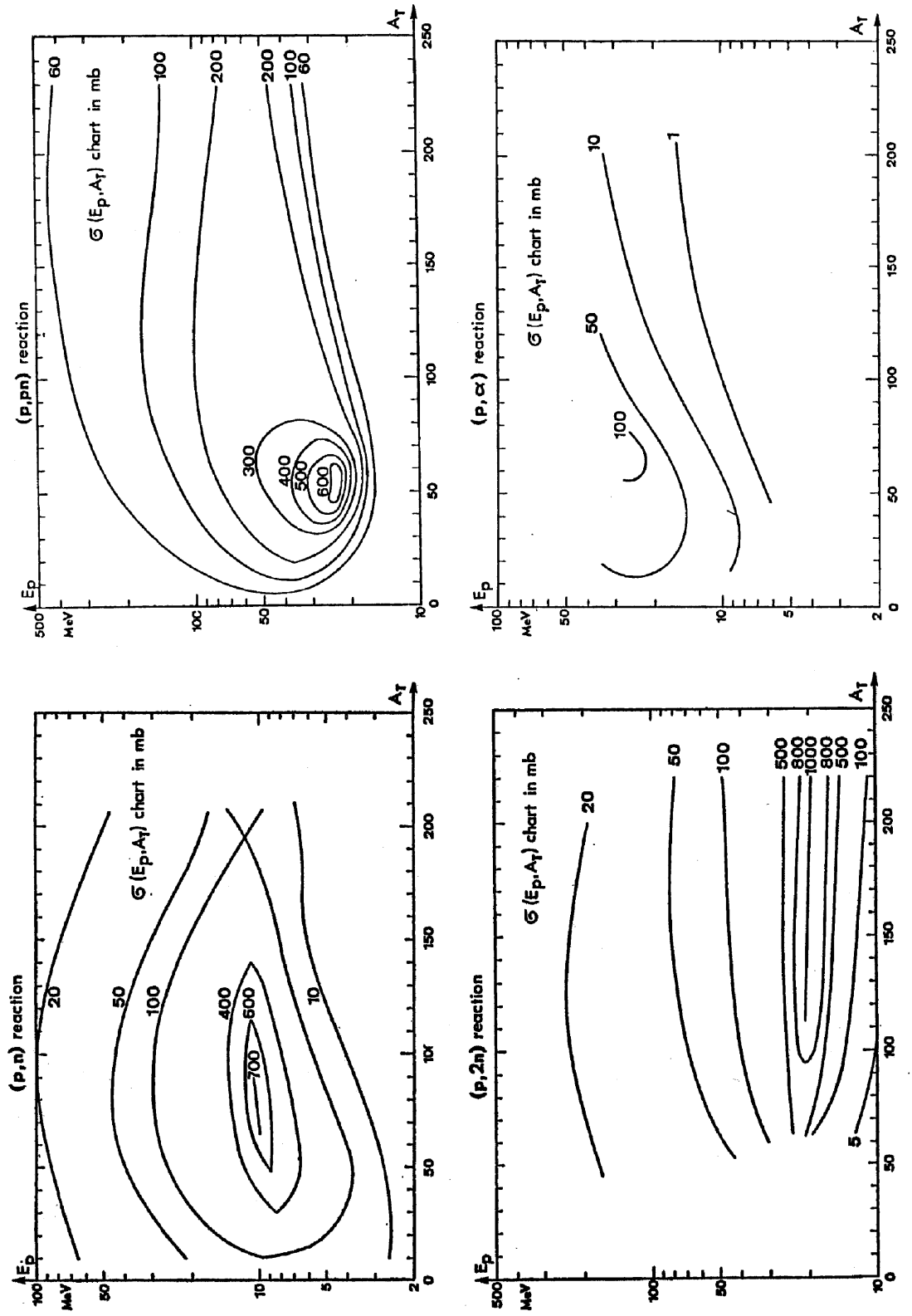

Fig. 7.5 Contours of equal cross section for proton-induced nuclear reactions (p, n), (p, 2n), (p, pn), and (p, α) as a function of particle energy, E_p , and target material mass number, A_T. The results have been smoothed in these plots. [Adapted from (Ba69).]

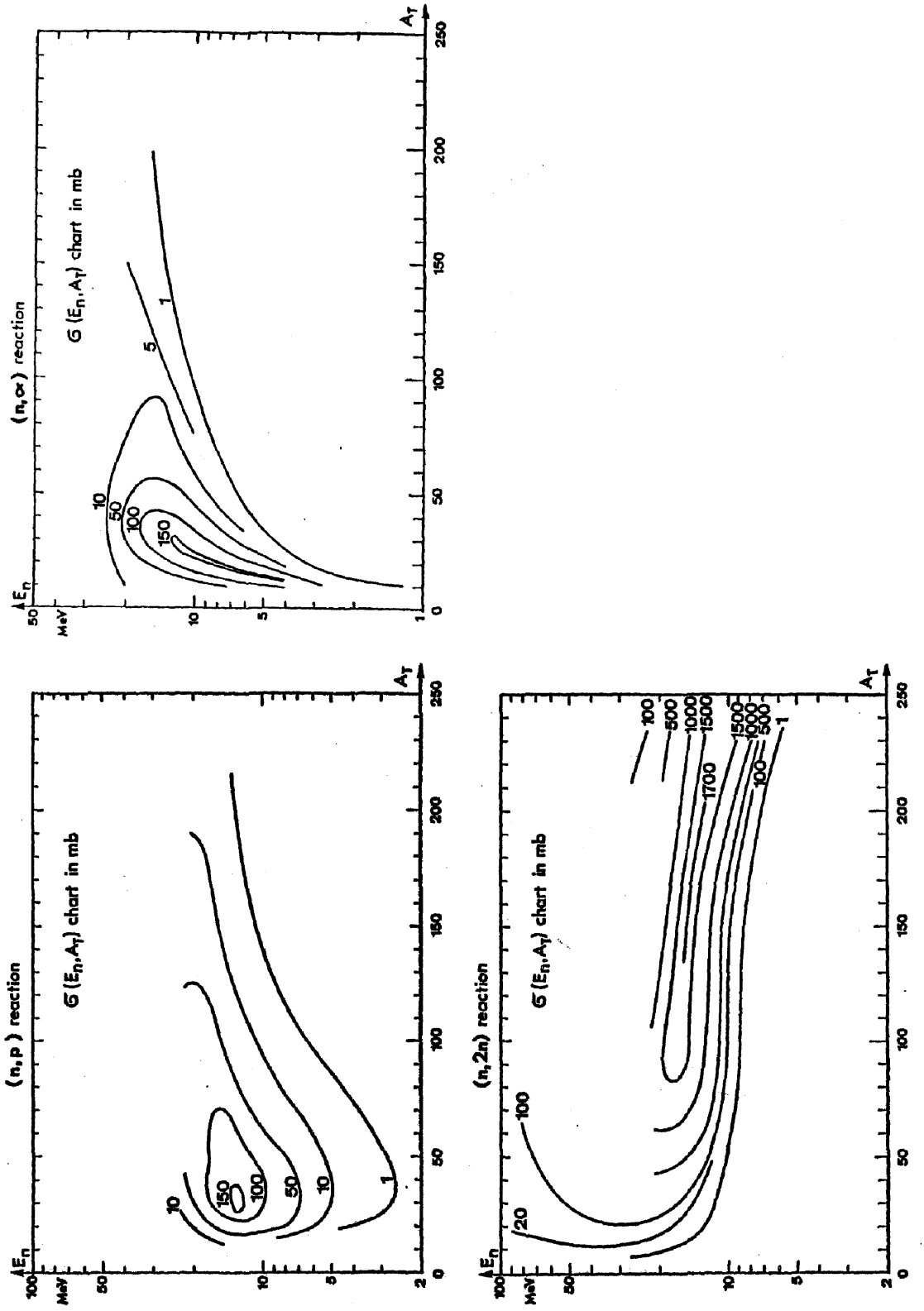

Fig. 7.6 Contours of equal cross section for neutron-induced nuclear reactions (n ,p), (n, 2n), and (n, α) as a function of particle energy, E_n , and target material mass number, A_T. The results have been smoothed in these plots. [Adapted from (Ba69).]

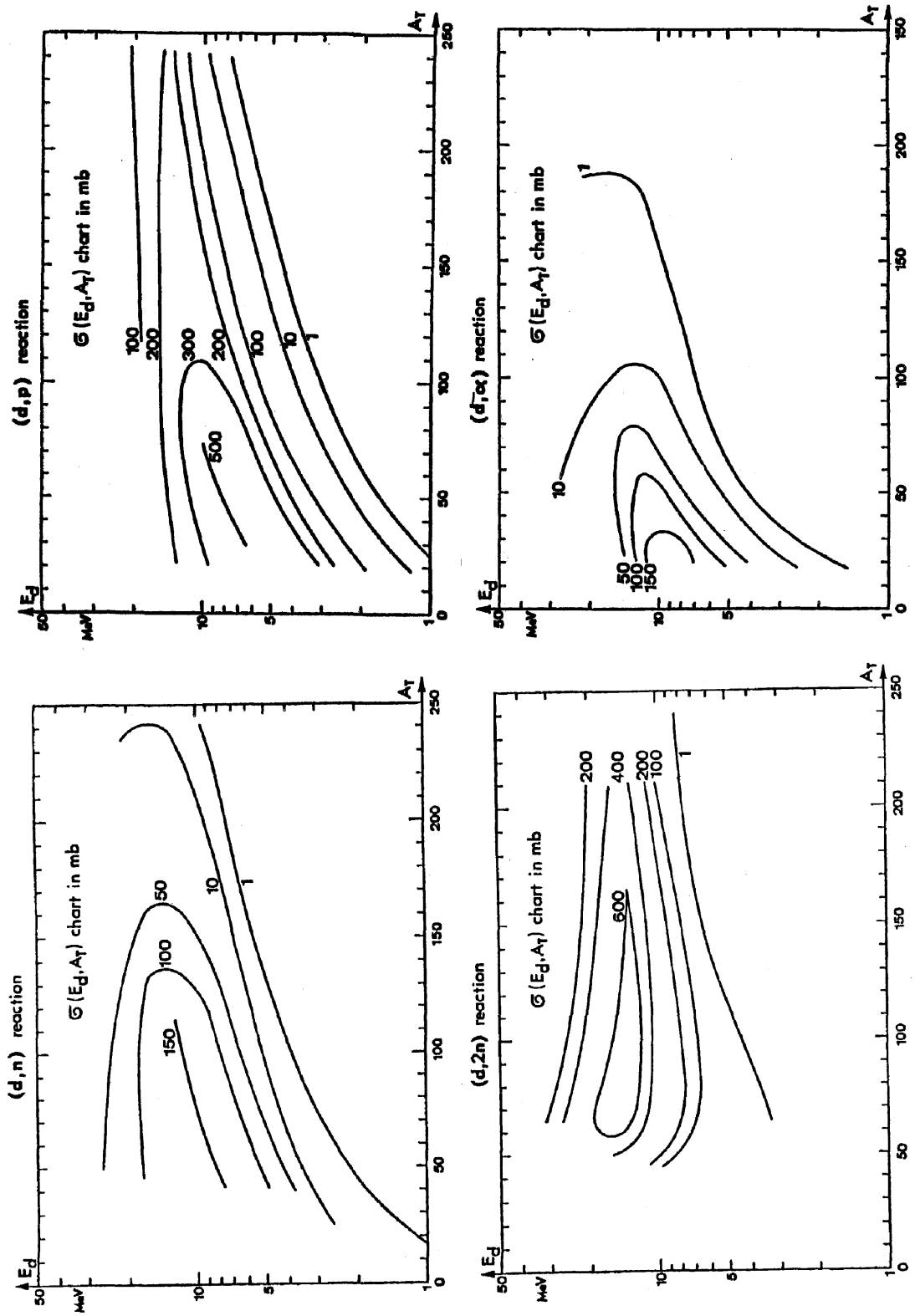

Fig. 7.7 Contours of equal cross section for deuteron-induced nuclear reactions (d ,n), (d, 2n), (d, p), and (d, α) as a function of particle energy, E_d , and target material mass number, A_T. The results have been smoothed in these plots. [Adapted from (Ba69).]

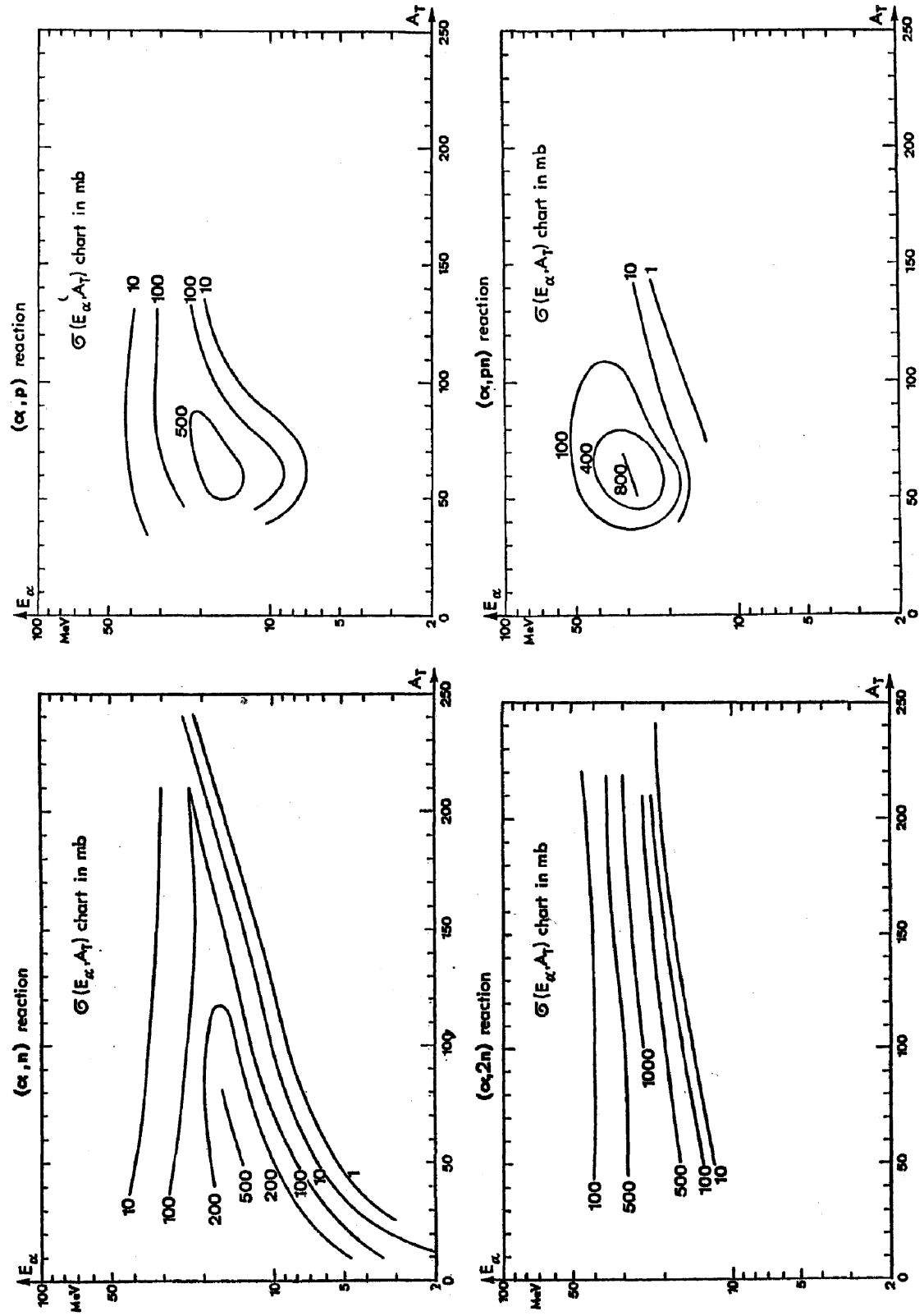

Fig. 7.8 Contours of equal cross section for α-particle-induced nuclear reactions (α, n), (α, 2n), (α, p), and (α, pn) as a function of particle energy, E_α, and target material mass number, A_T. The results have been smoothed in these plots. [Adapted from (Ba69).]

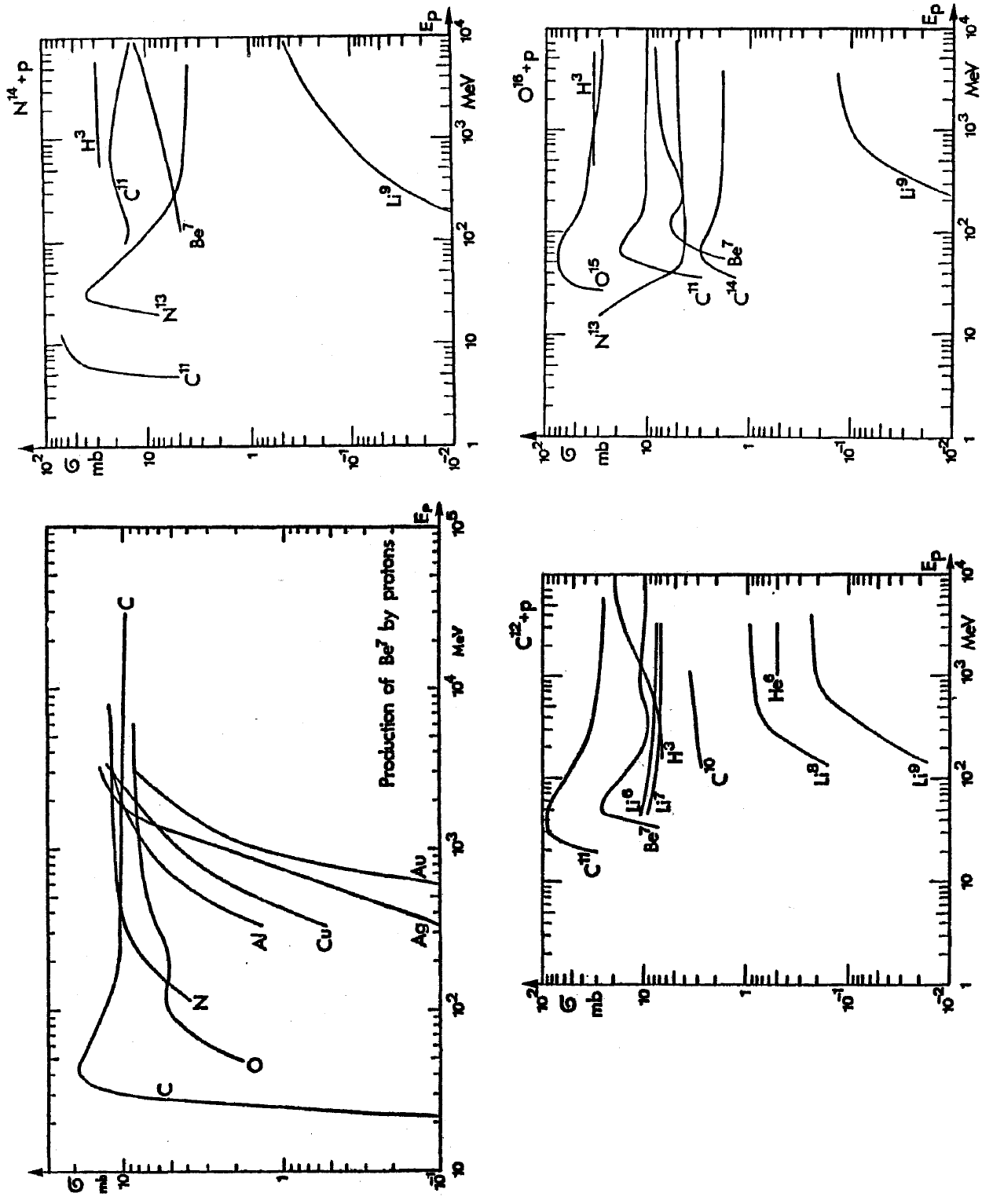

Fig. 7.9 Excitation functions for the production of various radionuclides by protons incident on some light targets. [Reproduced from (Ba69).]

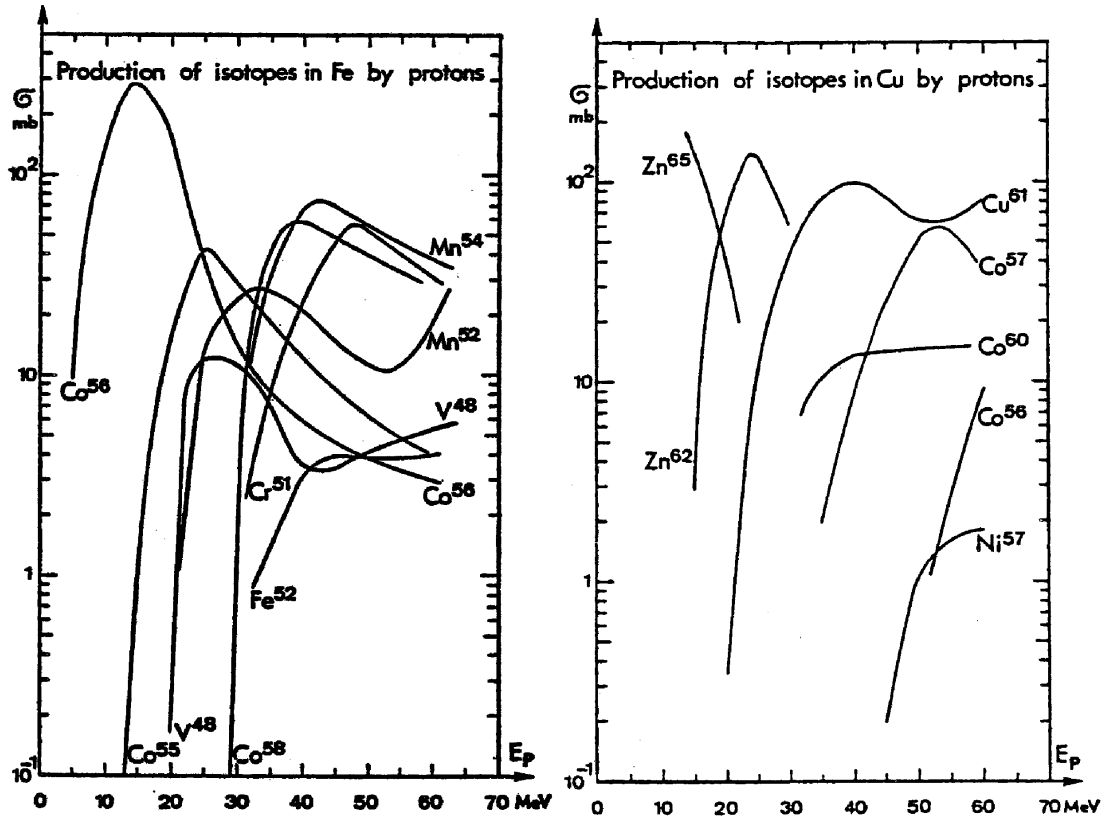

Fig. 7.10 Excitation functions for the production of various radionuclides by protons incident on iron and copper targets. [Reproduced from (Ba69).]

$\sigma(E_\gamma, A_T)$ where E_γ is the photon energy and A_T is the mass number of the target material. These data are intended to convey the general idea of the importance of various processes at different energies. Other data has also been provided concerning specific reaction processes at a variety of energies. These results are provided in Figs. 7.5, 7.6, 7.7, 7.8, 7.9, and 7.10. The results for the light elements (Fig. 7.9) are especially important for environmental radiation considerations while those for iron and copper targets (Fig. 7.10) are of great importance due to the universal presence of those elements in accelerator components.

Thick target yields of radionuclides for targets having a range of atomic numbers have been systematically studied by Cohen for a number of nuclear processes spanning the periodic table (Co78). Fig. 7.11 is a representative plot of the general features of such excitation functions of such nuclear reactions. Specific processes may vary considerably from this behavior since "resonances" at specific nuclear excited states have been ignored. Table 7.3 lists a variety of such nuclear reactions along with the range of values of energy above threshold at which the radioactivity production rate has risen to 0.1% of the saturation value and also the range of saturation values for the production of radioactivity. It is assumed that the target thickness comfortably exceeds the range of the incident ion and that the irradiation period greatly exceeds the half-life of the radionuclide of interest. For shorter bombarding periods, t_i,, one needs to multiply by the factor

[1 - exp(-λt_i)]. Over the energy range of these curves, the importance of activation by secondary particles is small compared to that encountered at higher energies.

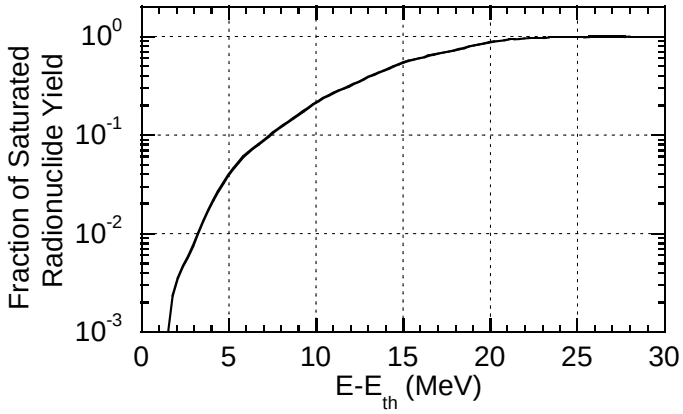

Fig. 7.11 Typical behavior of radionuclide production by (p,γ) or few-nucleon transfer reactions for energies not far above the reaction threshold, E_{th}. This behavior is typical of the nuclear reactions tabulated in Table 7.3. For detailed calculations, data related to specific reactions on specific target materials should be used. [Adapted from Co78).]

Table 7.3 Tabulation of generalized parameters for the production of radionuclides by means of low energy nuclear reactions which span the periodic table. The ranges of energies are listed at which the production yields are at approximately 0.1 per cent of the tabulated saturation values. The "high/low" values for the saturated activity are also given. [Adapted from (Co78).]

Reaction	0.1% Yield-low ($E-E_{th}$) (MeV)	0.1% Yield-high ($E-E_{th}$) (MeV)	Sat. Yield-low (μCi/μA)	Sat. Yield-high (μCi/μA)	Reaction	0.1% Yield-low ($E-E_{th}$) (MeV)	0.1% Yield-high ($E-E_{th}$) (MeV)	Sat. Yield-low (μCi/μA)	Sat. Yield-high (μCi/μA)
(p,γ)	4	9	3×10^2	10^3	(^{3}He,γ)	4	6	1	2
(p,n)	0	6	3×10^5	8×10^5	(^{3}He,n)	3	12	10^2	3×10^2
(p,2n)	1	4	3×10^5	10^6	(^{3}He,2n)	2	7	3×10^2	4×10^3
(p,3n)	1	6	3×10^5	10^6	(^{3}He,3n)	2	5	2×10^3	3×10^4
(p,4n)	5	8	2×10^5	10^6	(^{3}He,2p)	4	12	2×10^2	10^4
(p,5n)	5	10	10^5	2×10^6	(^{3}He,α)	6	14	2×10^2	10^3
(p,pn)	2	5	2×10^5	2×10^6	(^{3}He,p3n)	10	15	10^4	4×10^5
(p,p2n)	3	8	3×10^5	2×10^6	(α,γ)	10	13	3	20
(d,γ)	5	7	30	100	(α,n)	1	9	3×10^2	10^4
(d,n)	2	7	4×10^3	3×10^5	(α,2n)	1	4	5×10^3	4×10^4
(d,2n)	2	5	2×10^5	6×10^6	(α,3n)	1	6	3×10^3	7×10^5
(d,3n)	1	4	3×10^5	10^6	(α,4n)	5	8	3×10^3	4×10^4
(d,4n)	4	8	2×10^5	6×10^5	(α,5n)	5	8	10^4	3×10^5
(d,5n)	6	10	10^5	10^6	(α,p)	5	8	6×10^2	2×10^4
(d,p)	2	7	4×10^4	3×10^5	(α,pn)	3	12	3×10^3	8×10^4
(d,p2n)	2	10	10^5	2×10^6	(α,p2n)	5	15	3×10^3	7×10^4
(d,p3n)	8	15	10^5	2×10^6	(α,p3n)	7	15	10^4	3×10^4
(d,2p)	5	15	3×10^3	4×10^4	(α,2p)	5	10	10^2	3×10^3
(d,α)	4	7	10^4	3×10^4	(α,αn)	6	16	3×10^3	3×10^4
(d,αn)	5	15	2×10^4	10^5					

7.4.2 Methods of Systematizing Activation Due to High Energy Hadrons

For proton and ion accelerators of higher energy, the neglect of secondary reactions and the restriction to few- and multi-nucleon transfer reactions can become a serious deficiency in the accuracy of estimation of induced radioactivity because of the rise in importance of such processes as spallation. At about 40 MeV, only few-nucleon transfer reactions are available while at GeV energies, generally the entire periodic table of nuclides having mass numbers less than that of the target material becomes available. The variety of radionuclides that can be produced increases as one increases the bombarding energy because more thresholds are exceeded. As a general rule, at high energies ($E_O \approx 1$ GeV or greater), one must consider that all radionuclides in the periodic table that have mass numbers less than that of the material exposed to the flux of hadrons may be produced. Of course, many of these are of little significance due to short lifetimes and small production cross sections. In fact, the production cross sections for specific radionuclides often are nearly independent of the target element.

Table 7.4 gives a list radionuclides typically encountered in high energy proton accelerator installations and their half-lives. In this table only nuclides with half-lives between 10 minutes and 5 years are listed. Also, all "pure" β^- emitters are ignored. Pure β-emitters are those radionuclides that emit no γ-rays in their decays. Pure β^- emitters generally present minimal exposure hazards at accelerators as compared with γ-ray emitters in routine maintenance activities since the radionuclides are produced throughout the materials comprising accelerator components, with resultant self-shielding of the β-rays compared with the more penetrating γ-rays. In contract, β^+ emitters (positron-emitters) are included in this list due to the pair of 0.511 MeV photons that result from annihilation of the positrons with atomic electrons which readily occurs. Approximate thresholds and high energy cross sections for production of these radionuclides by protons, generally taken from the treatise by Barbier (Ba69) are also provided where available.

Table 7.4 Summary of radionuclides commonly identified in materials irradiated around accelerators. Approximate cross sections for their production at the high energy limit and approximate thresholds are given for selected radionuclides. [Adapted from (NC99) and (Ba69).]

Target Material	Radionuclides	Approximate Threshold (MeV)	Half-life	Production Cross Section (High Energy Limit) (mb)
Plastics & Oils	^{3}H	11	12.33 years	10
	^{7}Be	2	53.6 days	10
	^{11}C	20	20.4 minutes	20
Aluminum, Concrete	As above, plus			
	^{18}F	40	109.7 minutes	6
	^{22}Na	30	2.6 years	10
	^{24}Na	5	15.0 hours	10
Iron	As above, plus			
	^{42}K		12.47 hours	
	^{43}K		22.4 hours	
	^{44}Sc		3.92 hours	
	^{44m}Sc		2.44 days	
	^{46}Sc		84 days	
	^{47}Sc		3.43 days	
	^{48}Sc		1.83 days	
	^{48}V	20	16.0 days	6
	^{51}Cr	30	27.8 days	30
	^{52}Mn	20	5.55 days	30
	^{52m}Mn		21.3 minutes	
	^{54}Mn	30	300 days	30
	^{52}Fe	30	8.3 hours	4
	^{55}Fe		2.94 years	
	^{59}Fe		45.1 days	
	^{56}Co	5	77 days	30
	^{57}Co	30	270 days	30
	^{58}Co	30	72 days	25
Copper	As above, plus			
	^{57}Ni	40	37 hours	2
	^{65}Ni		2.56 hours	
	^{60}Co	30	5.27 years	15
	^{60}Cu		23 minutes	
	^{61}Cu	20	3.33 hours	100
	^{62}Cu		9.80 minutes	
	^{64}Cu		12.82 hours	
	^{62}Zn	15	9.13 hours	60
	^{65}Zn	0	244 days	100

A systematic way of handling the great multiplicity of radionuclides produced in accelerator components by high energy particles is highly desirable since it is often not practical to handle them all separately. Global properties of the distribution of radionuclides must be used. Sullivan and Overton (Su65) have treated this problem in an elegant manner that is restated here. The initial starting point is a modification of Eq. (7.8) describing the dose rate as a function of irradiation and cooling times, t_i, and t_c, respectively;

$$\delta(t_i, t_c) = G\phi\left[1 - \exp(-\lambda t_i)\right]\exp(-\lambda t_c)\,, \tag{7.12}$$

where $\delta(t_i, t_c)$ is the absorbed dose rate, ϕ is the flux density, and G is a collection of many contributing factors including the production cross section, the energy of the beam, the types of secondary particles produced, the isotopic composition of the irradiated component, the geometry, the energy of the γ-rays produced, and the attenuation coefficients for the γ-rays produced.

If the number of radionuclides produced by the irradiation which have decay constants in the interval between λ and $\lambda + d\lambda$ is represented by the differential, dm, then the corresponding increment in absorbed dose rate, $d\delta(t_i, t_c)$, is given by

$$d\delta(t_i, t_c) = G\phi\left[1 - \exp(-\lambda t_i)\right]\exp(-\lambda t_c)dm\,. \tag{7.13}$$

If it is assumed that the value of G is independent of λ, or its dependence on λ is small compared to other factors, then one can integrate[3]:

$$\delta(t_i, t_c) = G\phi\int_{\lambda_0}^{\infty} d\lambda \frac{dm}{d\lambda}\left[1 - \exp(-\lambda t_i)\right]\exp(-\lambda t_c)\,. \tag{7.14}$$

Here, λ_o is the shortest decay constant (longest mean-life) to be considered. Fig 7.12 is a plot of the number of radionuclides as a function of half-life, $t_{1/2}$, that have half-lives less than that particular half-life for several choices of atomic mass number, A. This corresponds to the distribution of radionuclides that could be produced in a target of mass number A irradiated by high energy hadrons. As one can see, these cumulative distributions are well-described for values of half-life between 10^{-3} and 10^{3} days by a function of the following form:

$$N(t_{1/2}) = a + b\ln(t_{1/2})\,, \tag{7.15}$$

[3]Taking this step implies the assumption that, on average, the radionuclide production cross sections under consideration are independent of both the half-lives and the particle energies. Somewhat remarkably, this approximation is a sufficiently accurate one.

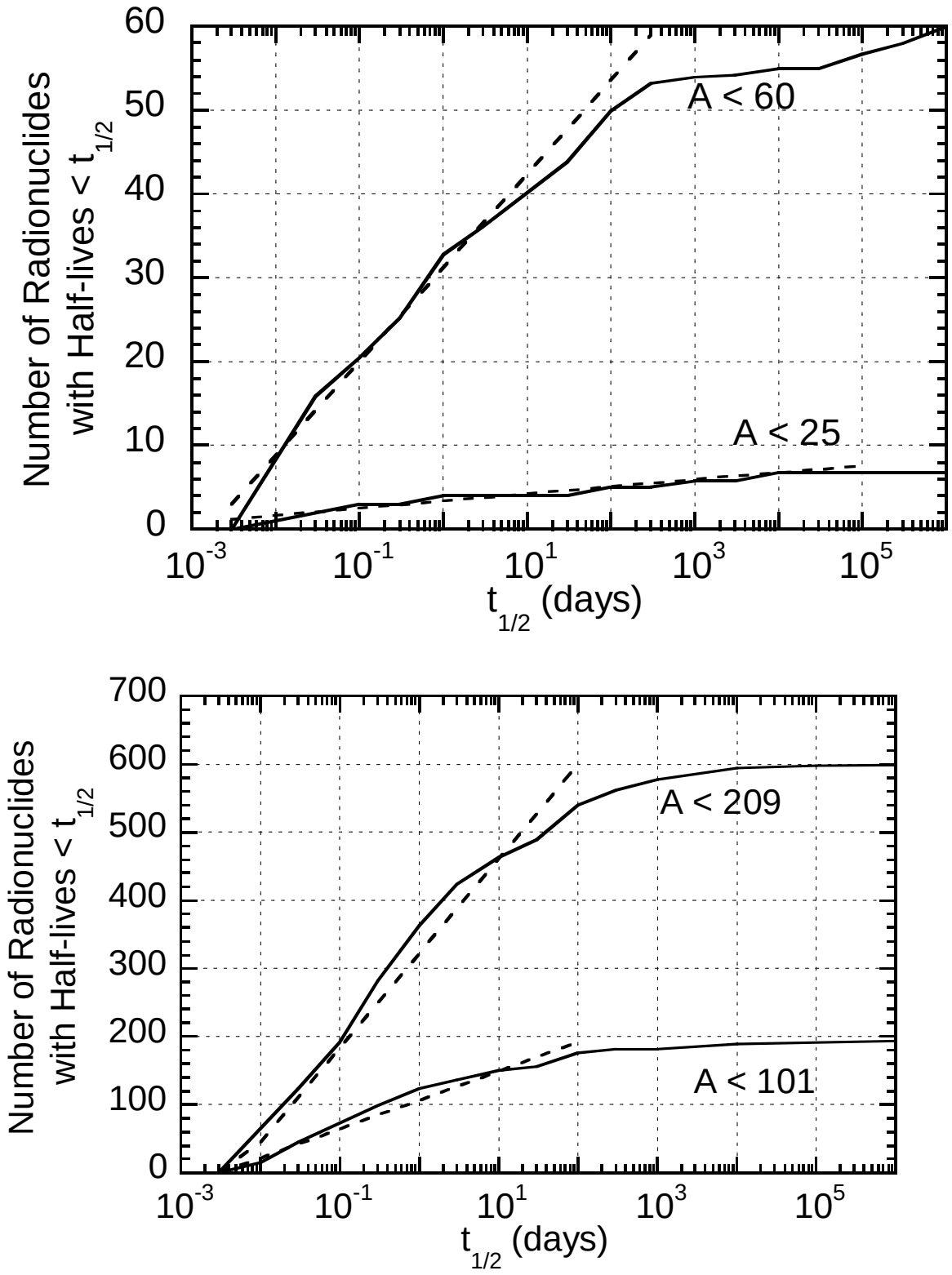

Fig. 7.12 Total number of radionuclides having half lives up to a given half-life as a function of half-life for target mass numbers less than those indicated. [Adapted from (Ba69).]

where $N(t_{1/2})$ is the number of radionuclides with half-lives less than the value of $t_{1/2}$ and a and b are fitting parameters.

Because of the one-to-one correspondence between values of $t_{1/2}$, τ, and λ, one can just as well write

$$m(\lambda) = a + b\ln\lambda\,, \tag{7.16}$$

where $m(\lambda)$ is the number of radionuclides with decay constants *greater* than λ for the material of concern. Thus,

$$\frac{dm(\lambda)}{d\lambda} = \frac{b}{\lambda}\,. \tag{7.17}$$

Substituting into Eq. (7.13), one gets

$$\delta(t_i,t_c) = Gb\phi\int_{\lambda_0}^{\infty}\frac{d\lambda}{\lambda}\left[1-\exp(-\lambda t_i)\right]\exp(-\lambda t_c) = Gb\phi\left\{\int_{\lambda_0}^{\infty}\frac{d\lambda}{\lambda}\exp(-\lambda t_c) - \int_{\lambda_0}^{\infty}\frac{d\lambda}{\lambda}\exp\left[-\lambda\left(t_i+t_c\right)\right]\right\}. \tag{7.18}$$

The changes of variables $\alpha = \lambda t_c$ (first term) and $\alpha' = \lambda\left(t_i + t_c\right)$ are helpful;

$$\delta(t_i,t_c) = Gb\phi\left\{\int_{\lambda_o t_c}^{\infty} d\alpha\frac{e^{-\alpha}}{\alpha} - \int_{\lambda_o(t_i+t_c)}^{\infty} d\alpha'\frac{e^{-\alpha'}}{\alpha'}\right\}. \tag{7.19}$$

Recognizing that the integrands are identical and simplifying by rearranging the limits of integration, we have

$$\delta(t_i,t_c) = Gb\phi\int_{\lambda_0 t_c}^{\lambda_0(t_i+t_c)} d\alpha\frac{\mathrm{e}^{-\alpha}}{\alpha}\,. \tag{7.20}$$

The integration results in a series expansion found in standard tables of integrals;

$$\int_{x_1}^{x_2}\frac{\mathrm{e}^{ax}dx}{x} = \left[\ln x + \frac{ax}{1!} + \frac{a^2x^2}{2\bullet 2!} + \frac{a^3x^3}{3\bullet 3!} + \ldots\right]_{x_1}^{x_2}. \tag{7.21}$$

Substituting,

$$\int_{\lambda_o t_c}^{\lambda_o(t_i+t_c)}\frac{\mathrm{e}^{-\alpha}d\alpha}{\alpha} = \left[\ln\alpha - \alpha + \frac{\alpha^2}{4} - \frac{\alpha^3}{18} + \ldots\right]_{\lambda_o t_c}^{\lambda_o(t_i+t_c)}. \tag{7.22}$$

Evaluating, one obtains

$$\delta(t_i, t_c) = Gb\phi\left[\ln\left(\frac{t_i + t_c}{t_c}\right) - \lambda_0 t_i + \ldots\right]. \tag{7.23}$$

Since λ_o approaches zero (corresponding to large lifetimes), the following is obtained:

$$\delta(t_i, t_c) \approx B\phi \ln\left(\frac{t_i + t_c}{t_c}\right), \tag{7.24}$$

where several constants are merged in the new parameter *B*.

7.4.2.1 Gollon's Rules of Thumb

Gollon (Go76) has further elaborated on these principles and determined some very useful "rules of thumb" for high energy hadron accelerators at which the extranuclear hadron cascade process produces the major fraction of the induced activity. Four rules are extremely useful for approximate radioactivity estimates:

Rule 1 This is equivalent to Eq. (7.10), repeated here for convenience:

$$\frac{dD}{dt} = 0.4\frac{S}{r^2}\sum_i E_{\gamma i} \tag{7.25}$$

where the summation is over all γ-rays present, including appropriate branching fractions if more than one photon is emitted per decay. If *dD/dt* is desired as an approximate absorbed dose rate in Gy h^{-1} at a distance *r* (meters) from a source strength *S* in GBq, the factor 0.4 becomes 1.08 x 10^{-4}.

Rule 2: In many common materials, about 50 % of the nuclear interactions produce a nuclide with a half-life longer than a few minutes. Further, about 50 % of these have a half-life longer than one day. Thus, approximately 25 % of the nuclear interactions (e.g., the "stars" discussed in Section 4.7.2) produce a radionuclide having a half-life exceeding approximately one day.

Rule 3: For most common shielding materials, the approximate dose rate *dD/dt* due to a constant irradiation is (see Eq. (7.24);

$$\frac{dD}{dt} = B\phi \ln\left(\frac{t_i + t_c}{t_c}\right). \tag{7.26}$$

In the above, the geometry and material dependent factor *B* can often be determined empirically, or by using *Rule 2*, while ϕ is the incident flux density. This expression appears to be valid also for intermediate energy heavy ion beams, for example at 86 MeV/nucleon (Tu84).

Rule 4: In a hadronic cascade, each proton or neutron produces about four inelastic interactions for each GeV of energy.

These rules can be illustrated by examples. In a short target of 1/10 of an interaction length, approximately 10 % of an incident beam of 10^{11} protons s^{-1} will interact. Assume this has been occurring for several months (long enough to reach saturation production for many radionuclides) at this constant rate. Using *Rule 2* in conjunction with the above rate, one determines that the decay rate after one day of the shutdown is 2.5 x 10^9 Bq (68 mCi). If each of these decays produces a one MeV γ-ray, then *Rule 1* will indicate an absorbed dose rate of 27 mrad h^{-1} ($\approx$ 0.27 mGy h^{-1} of absorbed dose rate) at one meter away.

Rule 3 can be used in such a calculation to predict the absorbed dose rate from a point source at some future time after beam shutdown. Furthermore, this rule is not restricted to "point" sources but can be used for more massive ones, with suitable adjustments to the geometry factors. Sometimes one can estimate the product $B\phi$ or use a measurement of the exposure or absorbed dose rate to determine it empirically for the purpose of using Eq. (7.26) to predict the "cooldown". In this way, *Rule 3* is also useful for extended shields irradiated by secondary particles from a well-developed cascade.

Rule 4 can be used to crudely estimate the activation of a beam dump by incident high energy particles when it is coupled with *Rule* 2. For example, a beam of 10^{12} 400 GeV protons s^{-1} (= 0.16 μA or 64 kW) produces a total of 4 x 400 x 10^{12} stars s^{-1} in a beam dump. If 25 % of these produce a radionuclide with a half-life > 1 day (*Rule 2*), then the total amount of the moderately long-lived radioactivity (at saturation) is

$$\frac{(0.25\,\text{atoms/star})(1.6\times10^{15}\,\text{stars/sec})}{3.7\times10^{10}\,\text{sec}^{-1}\,Ci^{-1}} = 10.8\,\text{kCi}\,. \tag{7.27}$$

At sufficiently large distance (say 10 meters), *Rule 1* could be used to calculate an absorbed dose rate at one meter assuming all decays are 1 MeV γ-rays;

$$\frac{dD}{dt} = 0.4(1\text{ MeV})\left(\frac{1.08\times10^{4}\text{ Curies}}{10^{2}\,\text{meter}^{2}}\right) = 43\text{ rads / hour}. \qquad (7.28)$$

A valuable quantity used to quantify the absorbed dose rate, *dD/dt* , at the surface of a thick target is the **danger parameter, D**, as developed by Barbier (Ba69) for a thick object irradiated by beam having a uniform flux density ϕ. If this source of radioactivity subtends solid angle Ω at the point of concern, then

$$\frac{dD}{dt} = \frac{\Omega}{4\pi}\phi\,\mathbf{D}. \qquad (7.29)$$

For contact with a semi-infinite slab of uniformly irradiated material, the fractional solid angle factor ($\Omega/4\pi$) has the intuitively obvious value of 1/2. The danger parameter has the physical interpretation as the absorbed dose rate found inside a cavity of arbitrary form embedded in an infinite volume of a material which has been uniformly irradiated by a unit flux density (one particle per second per square centimeter). Figures 7.13 give representative examples of plots of **D** for several elements and a few compounds. These curves thus can be used to predict cooling of various components around accelerators. Gollon (Go76) has also provided "cooling curves" for iron struck by high energy protons. These are given in Fig. 7.14 and include both calculations by Armstrong and Alsmiller (Ar73) and empirical measurements at the Brookhaven National Laboratory AGS, the Fermilab Main Ring Accelerator, and the Fermilab Neutrino Experimental Area target station.

Of course, one is often concerned with situations where the determination of ϕ in the danger parameter equation is not at all simple. For example, one can have activation in a large object where the hadronic cascade is contributing numerous hadrons at a variety of energies from a multitude of directions. Fortunately, important features of activation phenomena have little or no correlation with energy. The chief of these is evidenced by the excitation functions of various reactions. As seen in Figs. 7.9, 7.10, and 7.11, the cross sections rise just above the threshold and then, somewhere in the region of 10's of MeV above the threshold, a leveling-off occurs. Furthermore, in general the cross sections for production of radionuclides by neutrons and protons (and even other ions and particles) do not differ greatly from each other at the higher energies.

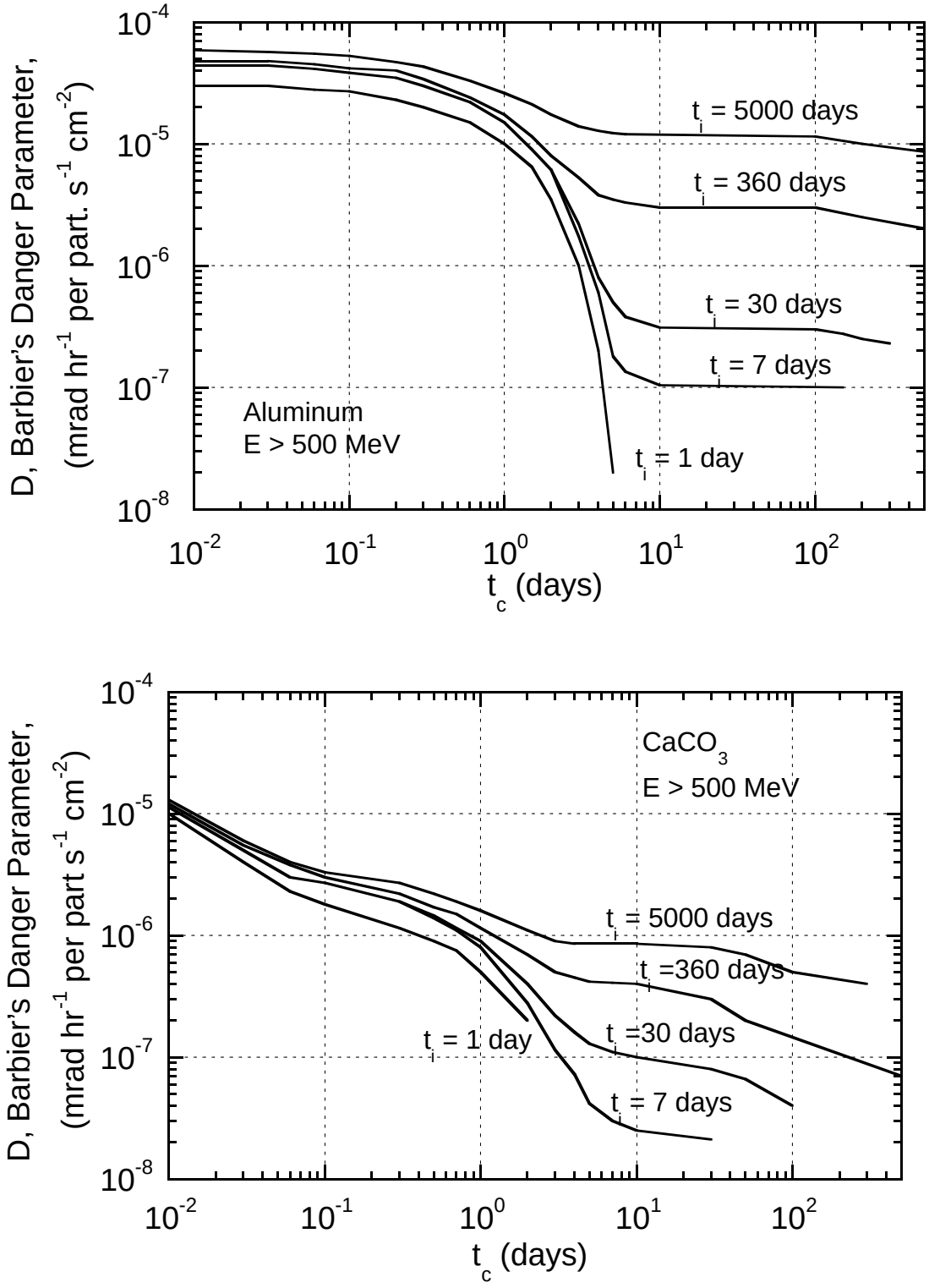

Fig. 7.13 Values of the Barbier danger parameter, **D**, for selected materials at a proton irradiation energy of 500 MeV. [Adapted from (Ba69).]

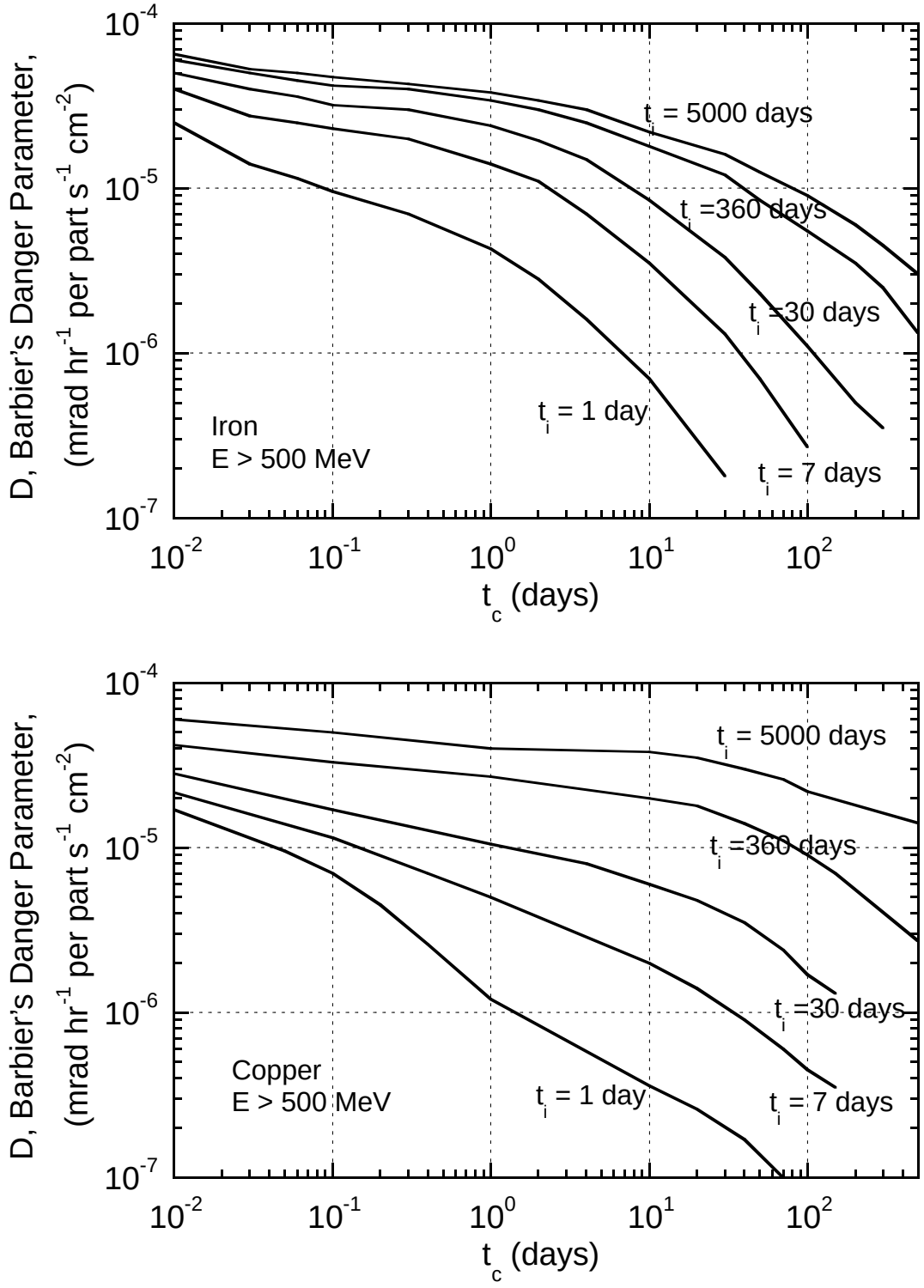

Fig. 7.13-continued.

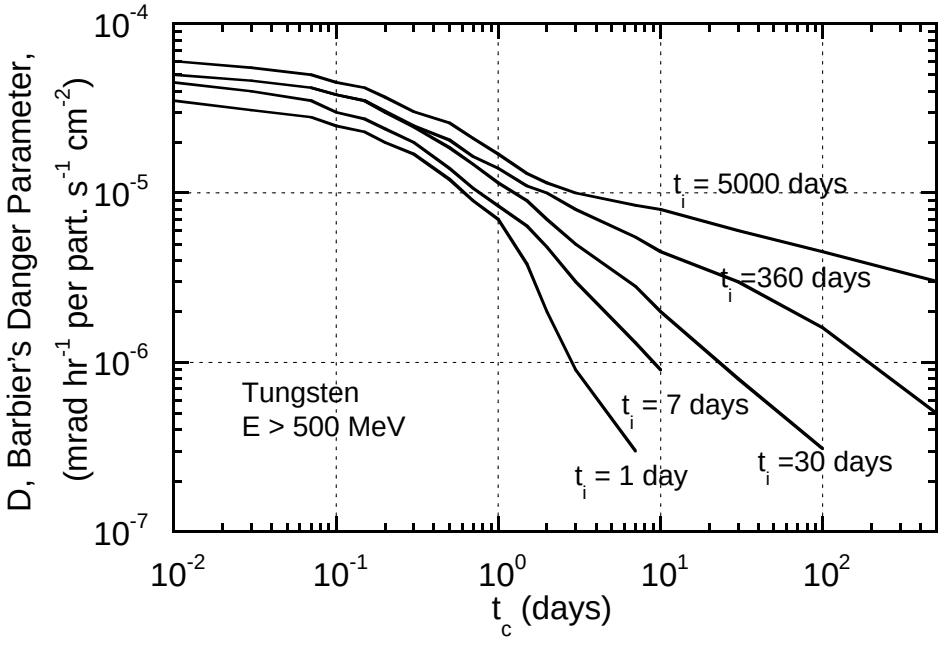

Fig. 7.13-continued.

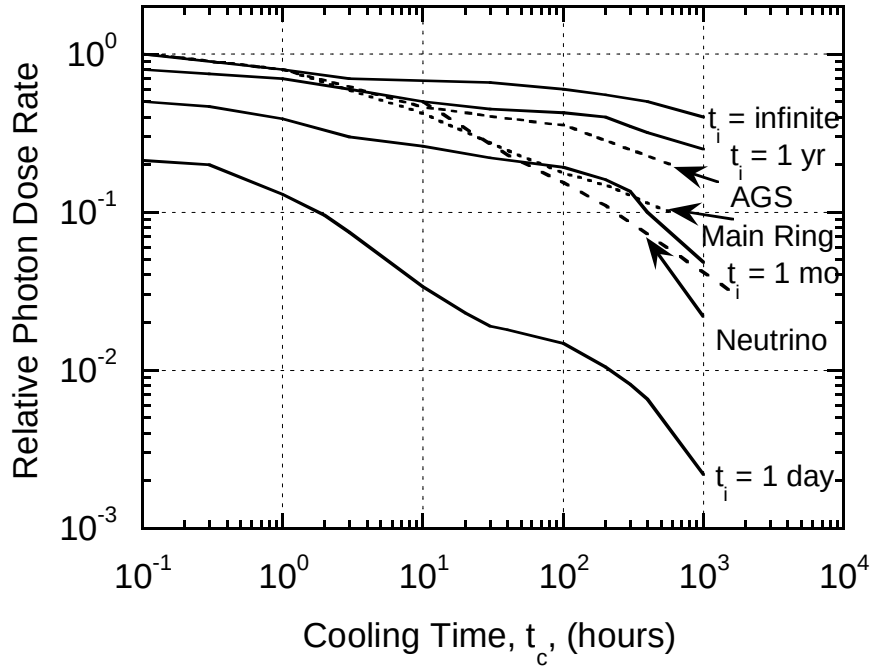

Fig. 7.14 Cooling curves for various irradiation times for iron struck by high energy protons as calculated by Armstrong and Alsmiller (Ar73). Also shown are the results of measurements. The one labeled "Main Ring", is the measured average cooling curve for the Fermilab Main Ring synchrotron after its initial three years of operation at 200-400 GeV. The curve labeled "Neutrino" is for a neutrino target station at Fermilab after eight months of operation at 400 GeV. The curve labeled "AGS" is for an extraction splitter in use for many years at the BNL AGS at energies up to 30 GeV. [Adapted from (Go76).]

7.4.3 The Utilization of Monte Carlo Star Densities in Activation Calculations

The "leveling-off" of the cross section as a function of energy has some very important implications the most important is the fact that for estimating activation, one can perform approximate calculations without performing integration over energy if one has some reasonable estimate of the flux above the reaction threshold of interest. An average effective cross section can then be used. Another feature of these excitation functions is the fact that the leveling off occurs in the region from a few 10's to a few 100's of MeV, precisely where relatively fast Monte Carlo hadron shielding calculations are available from several different codes (e.g., CASIM, FLUKA, HETC, and MARS).

It is often possible to relate the flux density of high energy hadrons (i.e., those with energies above the leveling off) to the star density, *S*, calculated from such Monte Carlo calculations through the relationship,

$$\phi(\vec{r}) = \frac{\lambda}{\rho}\frac{dS(\vec{r})}{dt} \ , \tag{7.30}$$

where $\phi(\vec{r})$, the flux density (cm^{-2} s^{-1}) at position vector at $\vec{r}$ is related to the rate of star density production $\frac{dS(\vec{r})}{dt}$ (stars cm^{-3} s^{-1}) at the same location[4]. ρ (g cm^{-3}) is the density and λ (g cm^{-2}) is the interaction length[5]. The value of $\phi(\vec{r})$ so determined could, in principle, be substituted into Eq. (7.29) for calculating absorbed dose rate due to residual activity using the Barbier danger parameter, **D**, if one were to make suitable adjustments in the solid angle. However, the limitation of this approach is the fact that the Monte Carlo cutoffs may introduce an energy (or momentum) cutoff (e.g., typically 300 MeV/c was used in CASIM) not necessarily matched to the reaction threshold. In order to calculate dose equivalent rates, Gollon (Go76) made detailed calculations and obtained the following formula:

$$\frac{dD(\vec{r})}{dt} = \frac{\Omega}{4\pi}\frac{dS(\vec{r})}{dt}\omega(t_i, t_c), \tag{7.31}$$

where $\omega(t_i, t_c)$ is related to the Barbier danger parameter, **D**. For iron, Gollon gives the following values for two useful situations:

$$\omega(\infty, 0) = 9 \times 10^{-6} \text{ rad h}^{-1}/(\text{star cm}^{-3}\text{ s}^{-1}) \tag{7.32a}$$

(infinite irradiation, zero cooling time), and

$$\omega(30\text{ d}, 1\text{ d}) = 2.5 \times 10^{-6} \text{ rad h}^{-1}/(\text{star cm}^{-3}\text{ s}^{-1}) \tag{7.32b}$$

(30 days irradiation, 1 day cooling time).

[4] This flux density is equivalent to the "star fluence" in Section 4.7.2.

[5] Once again, the adherence to traditional notation requires that care must be taken not to confuse interaction length with activity constant since they are customarily denoted by the same symbol, λ.

Estimates of other ω-values can be made by scaling results obtained by Armstrong and Alsmiller (Ar69a) and Gabriel and Santoro (Ga73) for selected values of t_i and t_c. This has been done by Cossairt (Co98) for three choices of values of t_i, and the results are shown in Fig. 7.15 for irradiated iron. Curves of this type should be used with some degree of caution. They can readily be used to predict the relative "cooling" rates of various components around accelerators with a fair degree of accuracy. Their use in the prediction of absolute dose equivalent rates due to activated accelerator components required additional care. To do this, the geometric configuration should be simple and well defined, the flux density of thermal neutrons should be a small component of the prompt radiation field, and the activation of other materials in proximity such as the enclosure walls should be taken into account. Cracks through the shielding materials can sometimes result in higher dose equivalent rates that are difficult to quantify. The interactions of thermal neutrons in concrete shielding can make a significant contribution to the dose equivalent rate. This phenomenon has been discussed by Armstrong and Alsmiller (Ar69b) and by Cossairt (Co96) and will be summarized in Section 7.4.4.

More generally, Gollon derived a simple relationship between dose rates involving cooling times different from "standard" ones for which values of **D** and ω are available. As stated previously, the dose rate after irradiation time t_i and cooldown time t_c is

$$\delta(t_i, t_c) = \sum_{\mu} \mathrm{A}_{\mu}\left[1 - \exp(-\lambda_{\mu} t_i)\right]\exp(-\lambda_{\mu} t_c), \tag{7.33}$$

where the summation over index μ includes all relevant radionuclides with the product of flux density and geometry factors being absorbed (and allowed to vary with radionuclide) in the quantity A_{μ}.

Rearranging, Gollon obtained

$$\delta(t_i, t_c) = \sum_{\mu} \mathrm{A}_{\mu}\left[\exp\{-\lambda_{\mu} t_c\} - \exp\left\{-\lambda_{\mu}(t_i + t_c)\right\}\right] =$$
$$\delta(\infty, t_c) - \delta(\infty, t_i + t_c). \tag{7.34}$$

Thus, the infinite irradiation curve can be used to determine any other combination of the times t_i and t_c. In fact, this formula may be used also with empirical results such as, for example, radiation survey data, in order to predict future radiological conditions.

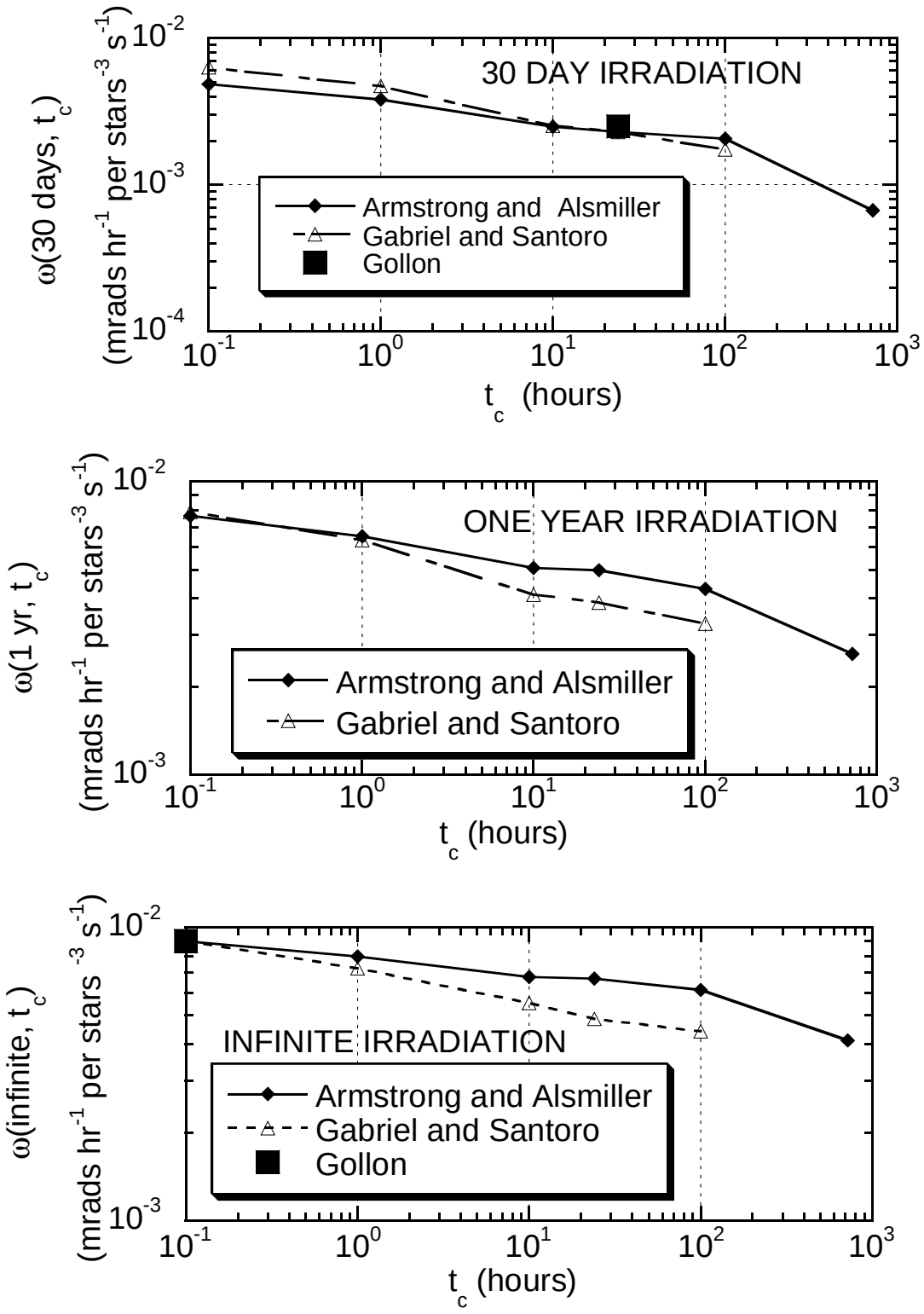

Fig. 7.15 Extrapolations of the cooling factor $\omega(t_i,t_c)$ from the work of Armstrong and Alsmiller (Ar69a) and Gabriel and Santoro (Ga73) compared with those of Gollon (Go76) for irradiated iron. [Reproduced from (Co98).]

A reliable method for connecting the production of "stars" in material (e.g., as calculated by a Monte Carlo code) to the production of atoms of some radionuclide is by the ratios of cross sections. Thus, at some point in space, $\vec{r}$, the rate of production of atoms per cm^3, $n(\vec{r})$, of some radionuclide is approximately given by

$$\frac{dn(\vec{r})}{dt} \approx \frac{\sigma_r}{\sigma_{in}} \frac{dS(\vec{r})}{dt} = \frac{\Sigma_r}{\Sigma_{in}} \frac{dS(\vec{r})}{dt}, \tag{7.35}$$

where one essentially scales the star density production rate (e.g., stars cm^{-3} s^{-1}) by the ratio of the production (reaction) cross section for the nuclide of interest, σ_r, to the total inelastic cross section σ_{in} or, equivalently, by the macroscopic cross section ratio (Σ_r/Σ_{in}). The phenomena will obey the usual activation equation. The reason this is *approximate* is due to the standard concerns about constancy of cross sections with energy, the lack of perfect "matching" of thresholds, etc.

7.4.4 Uniform Irradiation of the Walls of an Accelerator Enclosure

Somewhat special considerations may apply to the concrete shielding surrounding accelerators. As was seen before, ordinary concrete typically contains a partial density of 0.04 g cm^{-3} of sodium. This "typical" value varies a great deal due to the variety of minerals that might be present in local concrete. The significance of this seemingly small additive is that the naturally dominant isotope present is ^{23}Na. This nucleus has the relatively large thermal neutron capture cross section of 535 mb. Patterson (Pa58) determined that average thermal flux density, ϕ_{th}, in a concrete room is approximately given as follows:

$$\phi_{th} = \frac{1.25Q}{S}, \tag{7.36}$$

where Q is the number of fast neutrons produced per second in the enclosure and S is the inside surface area of the enclosure (cm^2). Thus, a substantial flux density of thermal neutrons can be present in an accelerator room and this flux can produce significant amount of ^{24}Na with its 15-hour half-life. The relatively high energy photon emitted in its decay (2.75 MeV) also can enhance the radiation hazard. Furthermore, while the dose due to activated components falls off radially with distance, if absorption by the air is not significant, the absorbed dose rate due to residual activation in an empty cylindrical room uniformly irradiated by such thermal neutrons is a constant. Thus, the dose equivalent rate anywhere inside the enclosure will be equal to the dose equivalent at the wall. This has been explicitly demonstrated for cylinders by Armstrong and Barish (Ar69b) and is also true for the interior of all mathematically well-behaved closed surfaces (Co96). This fact can readily be demonstrated by analogy to the Gauss Law in electrostatics[6] as follows by examining the situation in Fig. 7.16.

[6] The Gauss law of electrostatics has been treated in detail by Jackson (Ja75) and by Konopinski (Ko81).

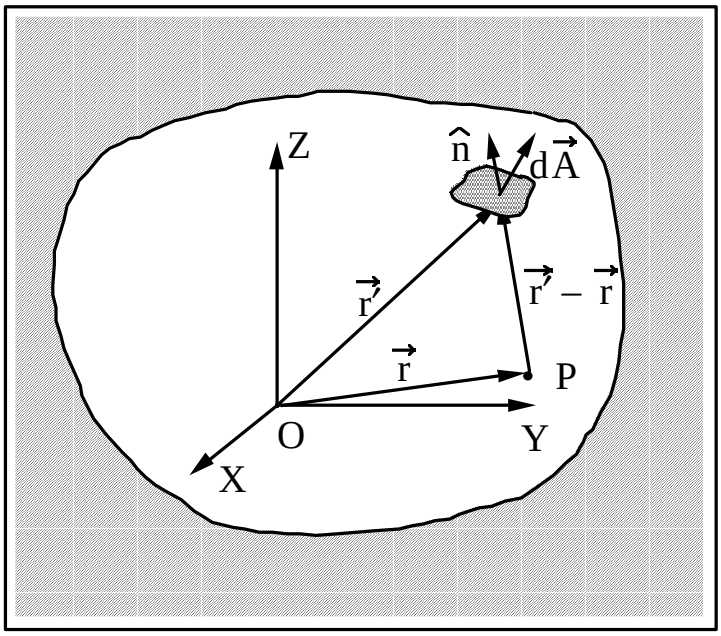

Fig. 7.16 Geometry for deriving relationship between a surface of uniform emission and the flux density at any point within it. [Reproduced from (Co96).]

Consider a simple, closed surface that emits an omnidirectional flux density of some particle ϕ_o (e.g., particles $cm^{-2}s^{-1}$) that is constant over the surface. One wants to calculate the flux density at some point in space *P* within the surface. *P* is located at radius vector $\vec{r}$. Consider further the contributions of the particles emitted by some elemental area $d\vec{A}$ at *P* where $d\vec{A}$ is perpendicular to the surface at coordinate vector $\vec{r}$. The solid angle subtended at *P* by $d\vec{A}$ is:

$$d\Omega = \frac{d\vec{A} \bullet \hat{n}}{\left|\vec{r}' - \vec{r}\right|^2} \tag{7.37}$$

where the unit vector $\hat{n}$ is given by

$$\hat{n} = \frac{\vec{r}' - \vec{r}}{\left|\vec{r}' - \vec{r}\right|} \ . \tag{7.38}$$

But the increment of flux at point *P* due to elemental area $d\vec{A}$ is given by:

$$d\phi = \frac{\phi_O}{4\pi} \frac{d\vec{A} \bullet \hat{n}}{\left|\vec{r}' - \vec{r}\right|^2} .$$

Thus,

$$d\phi = \frac{\phi_o}{4\pi} d\Omega \text{ and } \int_{4\pi} \frac{\phi_o}{4\pi} d\Omega = \phi_o . \tag{7.39}$$

In some situations it is been important to minimize the amount of sodium in the concrete ingredients in order to reduce exposures to individuals conducting maintenance on the accelerator. In fact, the phenomena described above has been noticed at accelerators and sometimes leads to "disappointment" in how little gamma-ray exposure rates are reduced when activated accelerator components are removed from enclosures with equally activated walls. For example, Armstrong and Barish (Ar69b) have calculated residual dose rates inside a cylindrical accelerator tunnel due to both the magnets and the concrete walls for 3 GeV protons incident on iron. These authors have also considered some other reactions that are capable of also producing ^{24}Na (spallation) that also must be included. The results are shown in Fig. 7.17 for the surface at the tunnel wall.

The discussion of the production of radioactivity continues in Chapter 8 with specific emphasis on environmental radiation protection.

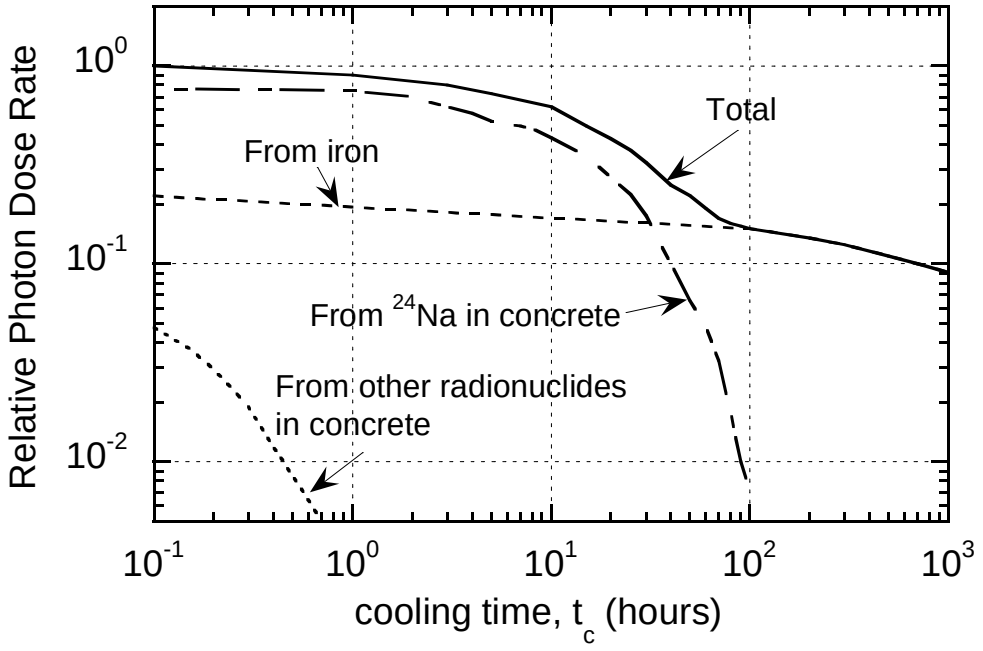

Fig. 7.17 Photon dose rate at surface of tunnel wall after infinite irradiation time for concrete containing one per cent sodium by weight. [Adapted from (Ar69b).]

Problems

1. A 1 mA beam of 30 MeV electrons is absorbed by an aluminum target. Calculate the saturation activities of all major radionuclides produced in the target. Assuming no self-absorption and an infinitely long irradiation period, what will the absorbed dose rate at a distance of 2 meters away immediately after beam shutdown and one hour later? The target can be assumed to be a point source for this estimate.

2. A copper beam stop has been bombarded with high energy hadrons for 30 days and exhibits a dose rate of 100 mrem hr^{-1} at 1 meter away 1 day after the beam is turned off. Maintenance work needs to be scheduled in the vicinity within the next 6 months. Using both Gollon's Rule No. 3 (as derived by Sullivan and Overton) and the Barbier Danger parameter curves, predict the cooling curve and determine when the dose rate is less than a 20 mrem hr^{-1} maintenance work criteria. Make a table of dose rate versus cooling time in days for both methods. How well do the two methods agree? (Hint: Use initial value of the dose rate to scale values of **D**.)

3. A 100 GeV beam (10^{12} protons s^{-1}) strikes the center of a large solid iron cylinder 30 cm in radius for 30 days. Use the star density curves from the Appendix B and the "ω" factors calculated by Gollon to estimate the residual dose rate after 1 day cooldown at contact with the side of the cylinder in the "hottest" spot. Using Gollon's third rule, how long must the repair crew wait to service this time in a contact radiation field of absorbed dose rate < 10 rad hr^{-1}?

4. A copper target is bombarded with high energy protons such that 10 stars per incident proton are produced. If the incident beam is 10^{11} protons s^{-1}, what is the specific activity (average) of ^{54}Mn that is produced after two years of operation? ^{54}Mn has a high energy spallation production cross section of about 20 mb in Cu. The target is a cylinder, 10 cm radius by 15 cm long. The half-life of ^{54}Mn is 312 days. Express the answer in both Bq cm^{-3} and Ci cm^{-3}. (Hint: This problem is best if the calculation is done at saturation and then corrected for the non-infinite irradiation time. Also, one needs to use the inelastic cross section given, for example, in Chapter 4.)